Title: Volcanism, Ozone Depletion, Global Warming, and the Drought of 2012

Authors: Peter L. Ward[1]*

Affiliations:

[1] U.S. Geological Survey, retired, Teton Tectonics, P.O. Box 4875, Jackson, WY 83001, USA.

* Correspondence to: E-mail: peward@wyoming.com.

Abstract: Global warming is greatest when and where ozone depletion is greatest. Ozone depletion allows solar ultraviolet energy that normally warms the stratosphere to penetrate to Earth's surface, cooling the stratosphere and warming Earth. Anthropogenic chlorofluorocarbons depleted total column ozone 3% over thirty years while the 1991 eruption of Pinatubo volcano depleted ozone an additional 6% within one year. Large explosive volcanic eruptions also form sulfuric-acid aerosols in the lower stratosphere that reflect and scatter solar radiation, causing net cooling. But small, effusive, basaltic eruptions deplete ozone substantially without forming significant aerosols, causing net warming. Ozone records from Toronto show that anthropogenic ozone depletion compounded by eruptions of Icelandic volcanoes Eyjafjallajökull (2010) and Grímsvötn (2011) played a major role in abnormal warming and drought during 2011-2012.

One Sentence Summary: Ozone depletion of 14% caused by man and small, basaltic volcanic eruptions moved heating from the stratosphere to Earth causing warming and drought.

Main Text: Greenhouse gas concentrations are essentially homogeneous around the globe and have been increasing monotonically over many decades. Greenhouse-gas theory, therefore, cannot explain directly well observed decadal to yearly changes in climate within specific geographic regions or more frequent changes in weather without appealing to short-term instabilities in oceanic and atmospheric currents and many other complexities within the climate system. The links between gas concentrations and climate change and between climate change and weather remain elusive.

Earth is warmed fundamentally by radiant energy from our Sun. Greenhouse gases may affect how rapidly Earth loses heat, but Earth's heat comes almost exclusively from solar energy. How much of this energy heats the atmosphere as opposed to how much heats Earth is determined by the chemical composition of the atmosphere and primarily by the distribution of ozone. Solar radiation varies ~1% in 11-year cycles, but total column ozone throughout the atmosphere has recently been depleted many tens of percent in late polar winters near the Arctic and Antarctic circles. In December, 2011, monthly average total column ozone above Toronto Canada at 43.6^{o}N averaged 14% below means observed during the 1960s as described below.

"From the time of Dobson's early measurements" in the 1920s, "it has been known that the total ozone amount undergoes large day-to-day fluctuations" (*1*) in specific regions such as 20% within 5 hours (*2*). It was also "discovered in the early years of ozone observations that there is a strong correlation between column ozone and meteorological conditions" (*1, 2*). These meteorological conditions have often been assumed to cause the ozone variations. In this paper we will explore evidence suggesting that large observed variations in ozone concentrations due primarily to changes in volcanism may be causing large changes in temperature of both the atmosphere and Earth, providing a clear mechanistic link between trace-gas concentrations, climate change and weather.

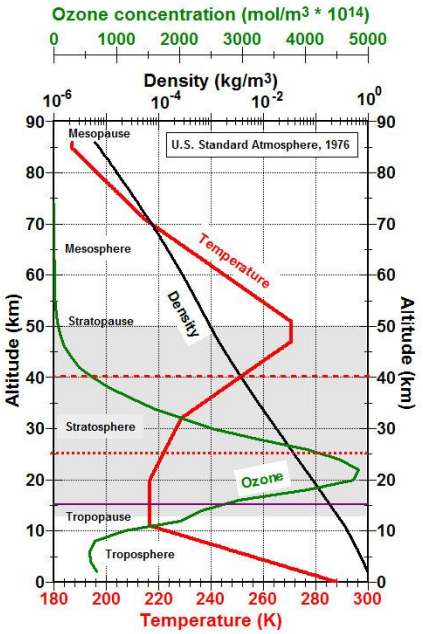

Fig. 1. The greatest warming in the atmosphere is between 35 and 60 km while the greatest concentrations of ozone are between 14 and 32 km. The profiles shown are for the U.S. Standard Atmosphere 1976 (*3*, *4*). Actual profiles vary with latitude, time of day, season and amount of ozone depletion. The dashed, dotted and purple lines correspond to altitudes of actinic flux calculations shown in Figure 2.

Photodissociation warms the atmosphere: The greatest warming of the earth system occurs all day, every day in maintaining the temperature at the stratopause (altitude ~50 km) typically ~55^{o}C warmer than the temperature at the tropopause (~13 km) (Figure 1) (*3*). The primary exothermic photochemical process at 50 km is the photodissociation of molecular oxygen (O_2) into two O(^{3}P) ground state oxygen atoms (*5*):

$$O_2 + h\nu(\lambda<242.4\ nm) \rightarrow O(^3P) + O(^3P)$$

where h is Planck's constant, ν (the Greek letter nu) is the frequency, hν is the energy (E) of radiation as a function of frequency based on Planck's postulate (E=hν), and λ is wavelength in nanometers (nm).

This equation expresses the fact that ultraviolet solar radiation with wavelengths less than 242.4 nm has sufficient energy (E>5.11 eV, electron Volts) to sever the O_2 molecular bond. Photodissociation is a particularly effective way to convert electromagnetic radiation into temperature because all of the oscillatory kinetic energy absorbed to break the O_2 bond is converted into translational kinetic energy of the two separating oxygen atoms and, according to the kinetic theory of gases, the temperature of a gas is equal to the average translational kinetic energy of all of its molecules and atoms times a constant.

The coolest part of the stratosphere is just above the tropopause where the atmosphere begins to warm with increasing altitude. This is also near the base of the ozone layer most concentrated between 14 and 32 km (Figure 1). The primary exothermic photochemical process at these lower altitudes is the photodissociation of ozone (O_3) to form molecular oxygen and an O(^{1}D) excited oxygen atom (*5*):

$$O_3 + h\nu(\lambda<310\ nm) \rightarrow O_2 + O(^1D)$$

$O(^1D)$ is highly reactive with water vapor (H_2O) to form the hydroxyl radical (OH) that oxidizes most pollutants in the atmosphere. Photodissociation of O_3 is driven primarily by ultraviolet radiation with $\lambda<310$ nm ($E>4.0$ eV) but formation of $O(^1D)$ can be caused by wavelengths of up to at least 411 nm. Quantum yields (fraction of molecules dissociated) as large as 0.08 have been observed for $\lambda=330$ nm (*6*). Matsumi et al. (*6*) find that "photodissociation from vibrationally excited ozone contributes approximately 25 to 40% to the overall $O(^1D)$ production rate for solar zenith angles from 40^o to 80^o respectively." Note the increase as ray paths lengthen toward the poles.

Longer wavelengths (463-1180 nm) throughout the range of visible light into the near infrared have sufficient energy to photodissociate ozone into O_2 plus the ground state oxygen atom $O(^3P)$ that reacts with O_2 to form ozone again (*6*). The net amount of ozone does not change, but continued photodissociation converts radiant energy into higher velocities of the molecules and thus higher temperature. Photodissociation of nitrogen dioxide (NO_2) can similarly produce $O(^3P)$ for $\lambda<397.8$ nm but with quantum yields >0.1 for $\lambda<\sim411$ nm (*7*).

Photodissociation caused by ultraviolet radiation ($\lambda<380$ nm) and some violet light (380-450 nm) plays a major role heating the whole atmosphere and heating a lower troposphere polluted by anthropogenic ozone and NO_2.

A dynamic balance: The thermal structure of the atmosphere is a dynamic balance primarily between the highest energy solar radiation to penetrate to a given altitude, i.e. the amount of energy that one molecule can absorb, the concentration of molecules that can absorb it, and the rapid increase in density (black line, Figure 1, logarithmic scale), i.e. the number of molecules whose translational kinetic energy must be increased to raise the temperature. Below the tropopause, convection, evaporation, and greenhouse gases begin to play more significant roles than in the stratosphere and above. Modern chemistry climate models include more than 45 photodissociation reactions and more than 100 gas-phase chemical reactions (*8, 9*), but the most important for warming center around nitrogen, making up 78% of the atmosphere, oxygen (21%), and ozone (0.00006%). Very small amounts of ozone are so important because in the presence of sufficiently energetic ultraviolet radiation, molecules of ozone are created, destroyed, and recreated through repetitive catalytic reactions (*10*).

The small amount of solar radiation in the extreme ultraviolet ($\lambda<124$ nm, $E>10$ eV) is typically absorbed above ~85 km altitude primarily through photoionization of N_2, O_2, and NO. In the mesosphere (Figure 1), wavelengths <242.4 nm photodissociate O_2 and there is ample O_2 to absorb all of the energy in these wavelengths above the troposphere.

The stratopause is the altitude where there are sufficient O_2 molecules at sufficiently low enough atmospheric densities being dissociated by sufficiently energetic ultraviolet radiation to cause the maximum increase in temperature (~55^oC). Lower in the stratosphere, oxygen atoms formed by photodissociation of O_2 combine with O_2 to form O_3 which is photodissociated by ultraviolet radiation as discussed above. At decreasing altitudes in the stratosphere, lower and lower energy radiation is still available, so that even though there are rapidly increasing numbers of O_2 and O_3 molecules, the mean translational velocities of particles of dissociated atomic oxygen decrease, limiting the temperature increase.

The tropopause is the border between high ozone mixing ratios in the stratosphere and low mixing ratios in the troposphere, which contains <10% of total column ozone (*2*). The average height of the tropopause varies from 16.6 km near the equator to 9 km near the poles

(*11*). Annual mean heights increased ~160 m from 1980 to 2004 while the lower stratosphere cooled ~2°C, the upper troposphere warmed ~0.1°C (*11*) and mean surface temperatures in the northern hemisphere rose ~0.5°C (*12*). When on June 19, 2004, total ozone measured at Montreal, Canada, increased 20% (70 DU, Dobson Units) in 5 hours, the height of the tropopause dropped from 13.5 km to 8.5 km (*2*).

Critical wavelengths: Atmospheric warming due to photodissociation is confined to a very narrow bandwidth (red shaded area, Figure 2) between the rapidly increasing absorptivity of ozone below 350 nm (black line) and the very rapidly increasing availability of solar energy above 290 nm (red and purple lines). The spectrum of radiation available from an overhead sun that normally reaches a given altitude is shown by actinic flux (AF) as estimated by Madronich (*13*).

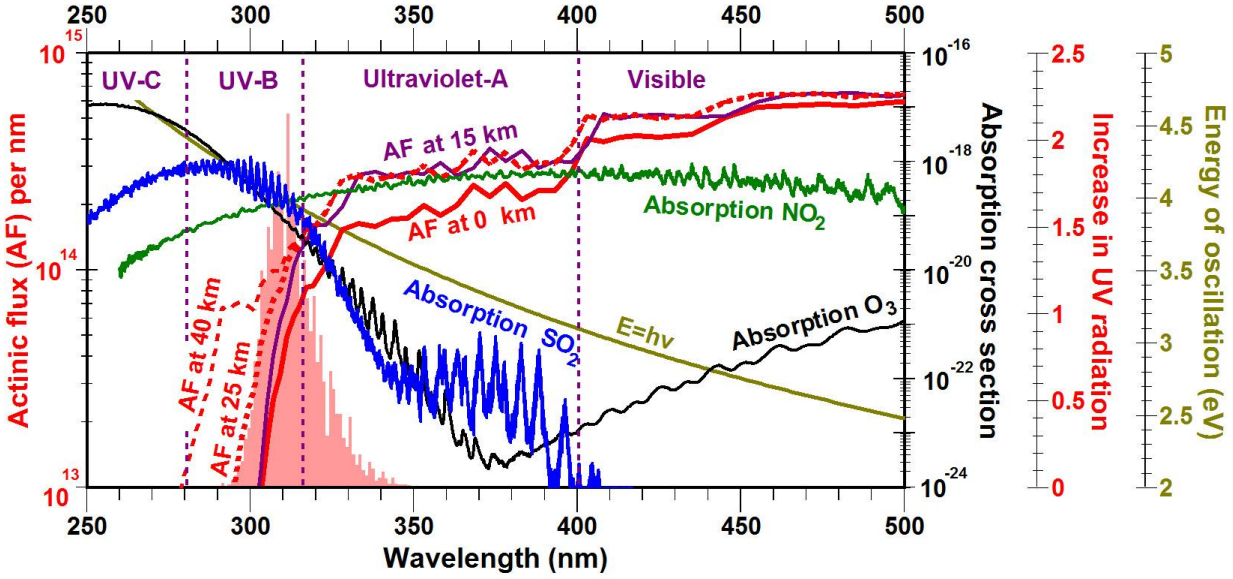

Fig. 2. A 1% decrease in total column ozone increases ultraviolet radiation reaching Earth's surface by ~34 mW m^{-2} between 290 and 340 nm (the red shaded area) when Sun is directly overhead (*14*). O_3, SO_2, and NO_2 absorb solar energy strongly at wavelengths <400 nm. Absorption by O_3 and NO_2 typically leads to photodissociation throughout the range of wavelengths shown. Actinic flux is photons cm^{-2} s^{-1}, absorption cross section is cm^2 per molecule, and increase in UV radiation is mW m^{-2} nm^{-1}.

Absorption by the ozone layer is essentially the difference in actinic flux at 40 and 15 km (dashed red and solid purple lines respectively in Figures 1 and 2). A 1% decrease in total column ozone will increase UV radiation at Earth's surface by 0.034 W m^{-2} for overhead Sun and 0.0092 W m^{-2} for a solar zenith angle of 70° (red shaded area) (*14*). These energy fluxes look small until multiplied by 70, the percent depletion of ozone often observed in the Antarctic Ozone Hole, yielding 2.4 W m^{-2} for overhead Sun and 0.64 W m^{-2} for a solar zenith angle of 70° that is closer to typical in sub-polar regions. These changes in energy flux, when integrated over Earth's surface, have the potential to explain at least some and possibly most of the observed warming believed caused by changes of <1 W m^{-2} (*15*) in the total energy budget of Earth's atmosphere.

This increase in ultraviolet energy will cause photodissociation of O_3 or NO_2 in the lower troposphere, be absorbed by SO_2, or be absorbed at Earth's surface. On land, much of the energy absorbed during the day is radiated back into the atmosphere at night. At sea, however,

ultraviolet radiation penetrates the ocean to depths >10 meters (*16*) and is thus more effective at heating the ocean than infrared radiation absorbed near the surface where much of the energy is lost back into the atmosphere at night. While volcanic aerosols may lower global temperatures as much as 0.5^{o}C for 2 to 3 years by reducing total solar radiation reaching Earth, the concurrent depletion of ozone allows more ultraviolet radiation that passes through the aerosols and most clouds to be absorbed efficiently by the ocean in areas with low ambient levels of pollution. The effect of this UV on surface temperatures would be small, but its effect on increasing ocean heat content could be substantial.

The fact that most ultraviolet C (100-280 nm) and ultraviolet B (280-315 nm) radiation is absorbed in the stratosphere and upper atmosphere is fortunate for life forms on Earth because radiation with λ<320 nm (E>3.87) has sufficient chemical energy to damage DNA, causing sunburn and skin cancer (*17*), fade colors in many materials, and even destroy the structural integrity of the surfaces of many materials. It also leads to the formation of vitamin D (*18*). Radiation from 295-320 nm is critical to life on Earth, is where the energies of solar radiation reaching the troposphere are highest (E=hν, olive line, Figure 2), is where absorption that causes photodissociation is very high for O_3 (black line)(*19*) and NO_2 (green line)(*19*), is where absorption by sulfur dioxide (SO_2) (blue line)(*20, 21*) is very high, and is where small changes in ozone depletion and tropospheric layers of pollution can have large effects on how much solar energy reaches the lower troposphere and Earth's surface. Note that absorption by O_3 and NO_2 is particularly strong because there is sufficient photochemical energy to cause electronic transitions and photodissociation at all wavelengths along a continuum (Figure 2) rather than along a limited number of spectral lines typical for greenhouse gases (Figures S1 and S2 in the Supporting Online Material (SOM)). Can we determine the relative importance of warming caused by ozone depletion versus warming caused by greenhouse gases?

The greatest warming observed on Earth: According to the *Intergovernmental Panel on Climate Change* (IPCC), global warming between 1976 and 2005 was most intense during June to August around the Western Antarctica Peninsula (*22*) and during December to February in North America, northern Europe and northwestern Russia (*23*), times and locations of greatest ozone depletion where there is still sufficient flux of solar radiation to cause warming. At Faraday/Vernadsky station on the Antarctic Peninsula (65.4^{o}S) increases in temperature were strongly correlated with decreases in total column ozone (*24*). Minimum monthly temperatures increased 6.7^{o}C from 1951 to 2003 (*24*), the greatest warming of this region in more than 1800 years (*25, 26*). Maximum monthly temperatures and ozone levels changed very little during summer months while summer surface temperatures of the Bellingshausen Sea rose 1^{o}C (*27*). Winter sea ice decreased 10% per decade and shortened in seasonal duration (*28*); 87% of the marine glaciers in this region retreated, many collapsing into the ocean following the loss of seven very large ice shelves (*28, 29*). The Circumpolar Deep Water of the Antarctic Circumpolar Current warmed (*28*). Warming of interior Antarctica was slowed by the high mean albedo (~0.86) of Antarctic snow, nearly twice the albedo of Arctic snow (*30*), and by the increase in solar zenith angle (decrease in solar flux) approaching South Pole.

In the Arctic, ozone depletion in early 2011 was unprecedented, exceeding 80% at altitudes of 18-20 km, comparable for the first time with the Antarctic ozone hole (*31*). The extent of Arctic sea ice, declining at >11% per decade since 1979 (*32*), reached a record low on September 16, 2012, nearly 50% lower than the average extent between 1979 and 2000 (*33*). Loss of ice in Greenland has been accelerating at a rate of 21.9 Gt/yr^2 (*34*). The Canadian Arctic

Archipelago has been losing ice at a rate of 61 Gt/yr (*35*). Average snow-covered area in the northern hemisphere decreased ~7% primarily since 1982 (*36*) when El Chichón erupted. The largest amount of global warming observed has been in the regions and at the times of greatest ozone depletion.

The longest continuous measurements of total column ozone have been made since 1927 at Arosa, Switzerland (black line, Figure 3) (*37, 38*). The dashed gray line with blue data markers shows from 1964 to 2009 the annual mean area-weighted total ozone deviation from the 1964-1980 means for northern mid-latitudes (30°N-60°N) scaled from -8% at the bottom of the figure to 10% at the top (*39*). Years of increasing or decreasing ozone are nearly identical at Arosa and for this area-weighted mean with small differences in amplitude. Thus the Arosa data provide a reasonable approximation for ozone changes throughout northern mid-latitudes since 1927.

Total column ozone at Arosa averaged ~331 DU until 1974, fell 9.4% to 300 DU by 1993 and began generally rising again until 2011. The long-term decrease in ozone has been reliably associated with an increase in concentrations of anthropogenic chlorine (green line, y-axis inverted) through discovery of the influence of stratospheric nitrogen oxides (*40*), chlorine catalyzed destruction of ozone (*10*), and the Antarctic ozone hole (*41*). The resulting Montreal Protocol on Substances That Deplete the Ozone Layer was signed beginning in 1987, leading to phasing out the production of chlorofluorocarbons and hydrochlorofluorocarbons and a decrease in tropospheric chlorine beginning in 1993. Long-term ozone concentrations are expected to return to late-1970's levels by 2040 (*42*).

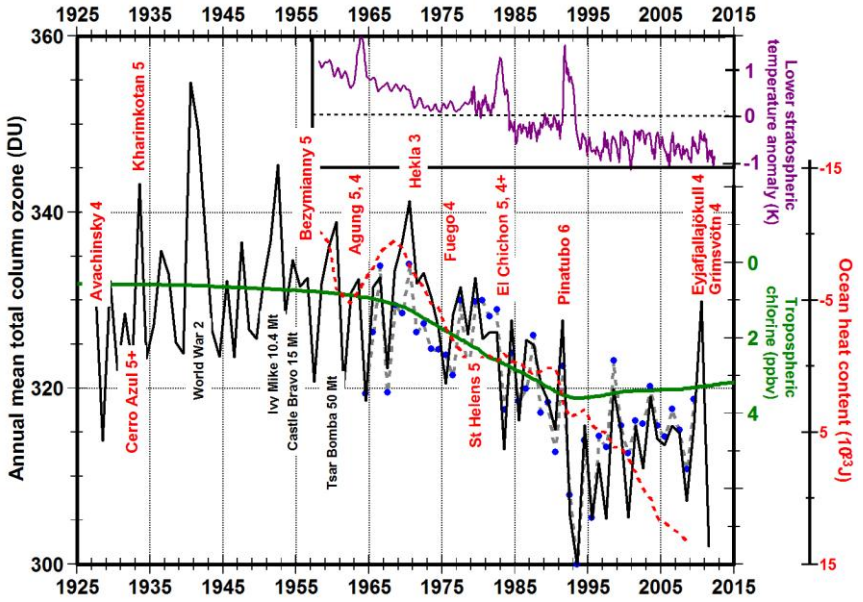

Fig. 3. Total column ozone (black line) peaks during years with major volcanic eruptions and then drops precipitously by more than twice as much during the following year causing a cooling in the lower stratosphere (purple line). The ozone data were measured at Arosa, eastern Switzerland (elevation 1820 meters) (*37, 38*). The names of the erupting volcanoes and the Volcano Explosivity Index (VEI) for each large eruption are labeled in red. The green line shows annual mean tropospheric chlorine with the y-axis inverted. The dashed red line with the y-axis inverted shows the increase of ocean heat content (*43*). The purple line shows the decrease in stratospheric temperature based on radiosonde data before 1979 (*44*) and satellite data since (*45*) smoothed with a seven-month centered running mean.

The largest short-term peak in annual mean total column ozone shown in Figure 3 occurred in 1940-1941, possibly related in some way to the onset of World War II. Large peaks in ozone also occur during years containing the three largest atmospheric nuclear tests (yield >10 Mt, megatons) (*46*). There is a peak in 1998 during one of the largest El Niños in history but no obvious peak in 1982-1983 during an El Niño with a comparably large multivariate ENSO index (*47*), although the latter observation may have been complicated by the eruption of El Chichón in 1982. But the most consistent short-term changes in ozone in Figure 3 are an apparent increase in ozone during the year of a volcanic eruption followed by a much larger depletion during the next few years.

The effects of volcanism on ozone: The largest eruption since 1912 was from Pinatubo in the Philippines during June, 1991, with a VEI (logarithmic Volcano Explosivity Index) of 6. An even larger ozone anomaly in March, 2010, is associated with the 100-times smaller basaltic fissure eruption of Eyjafjallajökull in Iceland (VEI=4). A slightly larger VEI=4 eruption of Grímsvötn, 140 km northeast of Eyjafjallajökull, occurred in May, 2011, compounding the amount of ozone depletion during 2011-2012. The amplitudes of these short-term ozone anomalies since 1990 are larger than the amplitudes of earlier volcanic anomalies before the global rise in tropospheric chlorine (green line, y-axis inverted). Anomalies appear associated with the eruption of Hekla in Iceland (1970, VEI=3) and with the larger eruptions of El Chichón in Mexico (1982, VEI=5 and 4+) and Agung in Bali (1963, VEI=5 and 4). Mt. St. Helens in Washington state (1980, VEI=5) had little effect on global temperature or ozone most likely because the main eruption was a blast of steam triggered by a landslide on the intruding volcanic plug (*48, 49*). The increase in ozone during the year of each major eruption is discussed in the SOM.

Depletion of stratospheric ozone during years following a volcanic eruption has been observed widely especially related to Pinatubo (*50, 51*). By January-April, 1993, total column ozone was 11 to 17% below preceding years throughout Canada with a peak loss of 30% at ~16 km (*52*). On average, total ozone decreased 8% in Europe, 5-6% in North America, Russia, and Asia but <2% in the tropics (*51*). Following Agung and El Chichón, the deceases were 5%, 2-3%, and <2% in these same regions. Following Pinatubo, lower tropospheric warming of up to 3^{o}C during the winter was observed throughout the more northerly parts of the northern continents (*53*), the parts with greater depletion of ozone. Related major changes in atmospheric chemistry are well documented by a 45% drop in total column NO_2 measured at Jungfraujoch, Switzerland, beginning five months after the Pinatubo eruption and returning to normal with an e-folding time of two years (*54*), a 40% decrease in NO_2 column observed above New Zealand (*55*), and substantial increases in HNO_3 concentrations due to heterogeneous conversion of N_2O_5 (*56-58*).

The observed ozone depletion (black line, Figure 3) was accompanied by cooling of the stratosphere (purple line) occurring mostly "as two downward 'steps' coincident with the cessation of transient warming after the major volcanic eruptions of El Chichón and Mount Pinatubo" (*59*) based on satellite measurements since 1979 and a similar downward step following the eruption of Agung volcano in 1963 (*60*) based on radiosonde temperature data.

Observed ozone depletion has traditionally been explained by the new aerosols formed in the lower stratosphere providing substantial new surfaces for heterogeneous chemical reactions to form ozone-destroying chlorine at cold temperatures (*61-63*). Yet water vapor (H_2O), the most

voluminous gas erupted from volcanoes, is the primary source of OH radicals that catalytically destroy ozone in the stratosphere (*58, 64, 65*). Volcanoes also erupt megatons of halogens (*58*), primarily chlorine and bromine (*66-68*) and only one halogen molecule can destroy >100,000 molecules of ozone (*10*). During explosive eruptions, many of these halogens appear to be removed immediately from the eruptive cloud in condensed supercooled water (*69*). But effusive, basaltic eruptions such as Eyjafjallajökull and Grímsvötn do not form significant eruption columns that remove halogens and that create aerosols in the stratosphere. They typically involve 10-100 times more volatiles per cubic kilometer of magma than explosive eruptions caused by more chemically evolved magmas (*70-72*). Ozone depletion is substantial within the plumes of erupting volcanoes; detailed observations imply that "the most likely cause for the observed rapid and sustained O_3 loss to be catalytic reactions with halogen, mainly bromine, radicals" (*68*). "Recent field observations have shown that even the plumes of quiescently degassing volcanoes are chemically very active containing halogens that modeling shows cause ozone depletion (*73*).

Volcanic eruptions are typically followed a year later by ~6% depletion of ozone averaged throughout the year (Figure 3). How do these short-term effects of volcanism compare to the longer-term effects of anthropogenic chlorofluorocarbons? The green line for chlorine is inverted and has been scaled so that the increase in anthropogenic tropospheric chlorine from 1965 to 1993 has approximately the same rate of change as the corresponding long-term decrease in ozone as expected by current theory. This visual fit suggests that depletion of ozone following the Pinatubo eruption (~20 DU) was twice as large as the depletion due to chlorofluorocarbons since 1960 (~10 DU) and that it takes more than a decade for ozone concentrations to return to pre-eruption levels. Large, explosive volcanic eruptions are well known to form sulfuric acid aerosols in the lower stratosphere that reflect, scatter, and absorb solar radiation, causing cooling at Earth's surface of ~0.5^{o}C over three years. These explosive eruptions also deplete ozone causing warming that lasts 3 to 5 times longer than the aerosols, but the cooling effects of the aerosol predominate. The much less explosive but much more numerous basaltic effusive eruptions such as Eyjafjallajökull and Grímsvötn as well as quiescently degassing volcanoes (*73*) do not form significant aerosols in the lower stratosphere so that ozone depletion and related warming are dominant.

Warming and drought in 2011-2012: The blue line in Figure 4A shows the average monthly total column ozone measured above Toronto, Canada, averaged for the years 1961 through 1970 when anthropogenic tropospheric chlorine had only increased 16% from levels in 1925 towards peak levels in 1994 (green line, Figure 3). The green line in Figure 4A shows average monthly column ozone for 2009 when anthropogenic chlorine had decreased 9% from its peak value. Note that ozone depletion is greatest between December and May, the months of greatest warming in the northern hemisphere reported by the IPCC (*23*). According to theory, the mean change in radiative forcing between the 1960s and 2009 caused by ozone depletion should be directly proportional to the area between the blue and green lines.

The solid red line includes both the increase in ozone during February preceding the first eruption of Eyjafjallajökull in March, 2010, discussed in the SOM, and subsequent depletion. The dashed red line shows total ozone in 2011 including depletion due to Eyjafjallajökull and increases and decreases related to the eruption of Grímsvötn. The double red line shows ozone levels in 2012. Note that since November 2011, the times when monthly maximum temperature

records have been set throughout central North America (*74*), ozone was depleted as much as 14% below mean values in the 1960s.

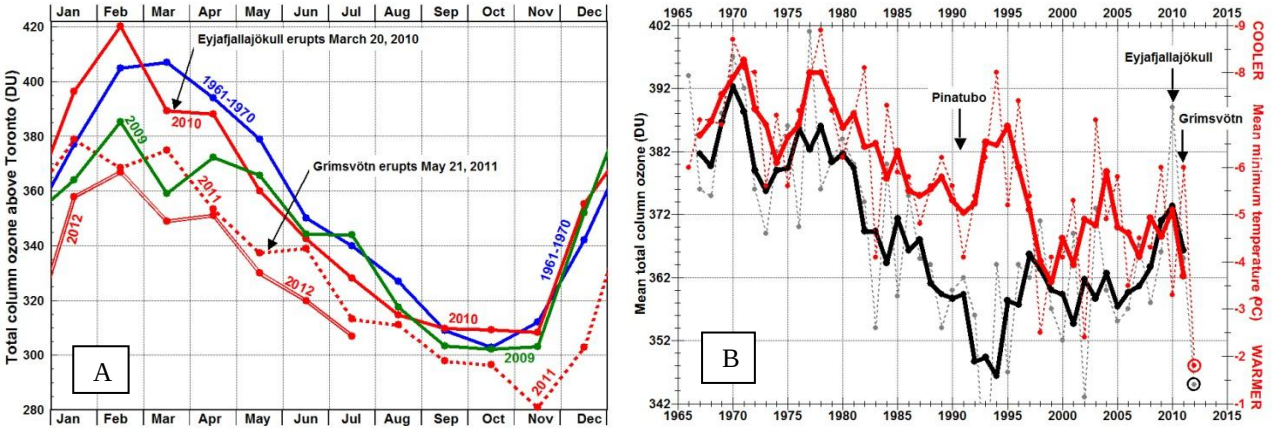

Fig 4. A. Total column ozone above Toronto, Canada, reached a minimum in November, 2011, 12% below the average for Novembers in 1961 through 1970 and has remained unusually low into July 2012. Data are from Environment Canada and the University of Toronto (*75*). B. When mean total column ozone measured during the months of December through April in Toronto Canada (black line) decreases, mean minimum temperature for the same months typically warms (red lines, y-axis inverted). The dashed lines show annual means; the solid lines are smoothed using a 3-point centered running mean. Temperature measured at the Toronto Airport by Environment Canada (*76*).

The dashed black line in Figure 4B shows the average for each year of the monthly mean total column ozone above Toronto averaged over four consecutive months from December through April; the dashed red line (y-axis inverted) shows the same average for monthly mean minimum temperatures. The solid lines are the same data smoothed using a 3-month symmetric running mean. A substantial decrease in ozone is typically but not always associated with an increase in minimum temperature except in 1992-1995 when aerosols in the lower stratosphere following the June, 1991, eruption of Pinatubo decreased radiation from the Sun as much as 2.7±1.0 W m^{-2} during August and September decaying exponentially to negligible values by 1995 (*77*). Note the extremely low ozone and high temperature in early 2012 (circled data points, lower right).

These data suggest that depletion of ozone due to the eruption of Eyjafjallajökull in 2010 and Grímsvötn in 2011 supplemented anthropogenic depletion leading to extreme ozone depletion and the resulting extreme temperatures and drought observed throughout central North America during late 2011 and 2012 and the highest sea surface temperatures ever recorded on the continental shelf off the northeastern United States during the first half of 2012 (*78*). The drought of 2012 approached the intensity of the great Dust Bowl droughts of 1934 and 1936 when a highly unusual sequence of seven VEI 4 and 5 eruptions occurred from 1931 through 1933 in Indonesia, Japan, Kurile Islands, Kamchatka, Alaskan, Guatemala, and Chile (*79*).

Recent warming and drought might be enhanced by the fact that November, 2011, had the largest number of sunspots per month since October, 2002 (*80*), and ultraviolet insolation increases four to six times more than broadband irradiance during solar cycles (*81*). In 1933 and 1934, however, the numbers of sunspots per month were relatively low until late in 1936.

Absorption without photodissociation does not appear to cause substantial global warming: Annual mean surface temperatures in the northern hemisphere (red line, Figure 5) (*12*) increased during the 1930s, cooled during the 1940s, remained relatively constant until 1975, rose rapidly until 1998 with a net temperature increase of ~0.8^{o}C, and have remained relatively constant until 2011 (*82*).

Total tropospheric chlorine caused by anthropogenic chlorofluorocarbons (green line) (*42*) increased rapidly from 1970, reached a peak in 1993 due to implementation of the Montreal Protocol and continues to decline slowly. Annual mean total column ozone (O_3, black line, y-axis inverted) fell rapidly from 1971 to 1995 and has been recovering slowly until the volcanic eruptions in 2010 and 2011. A slight delay after changes in chlorine concentration is expected since most ozone is formed above the tropics and circulates slowly to high latitudes where most ozone destruction occurs during winter associated with polar stratospheric clouds.

The primary time delay in the atmospheric system involves the heat capacity of the ocean covering 71% of Earth. A mere 3.2 meters of the ocean holds as much heat as the whole atmosphere yet the average depth of the ocean is 3800 meters (*83*). The observation that ocean surface temperature rose ~5 years after the decrease in ozone is in the range of calculations by Hansen et al. (*84*) for a 3.5-year e-folding time for warming the ocean if the equilibrium temperature of Earth suddenly increased a small amount and a 10-year e-folding time taking into account an ocean with a 100-meter-thick mixed-layer.

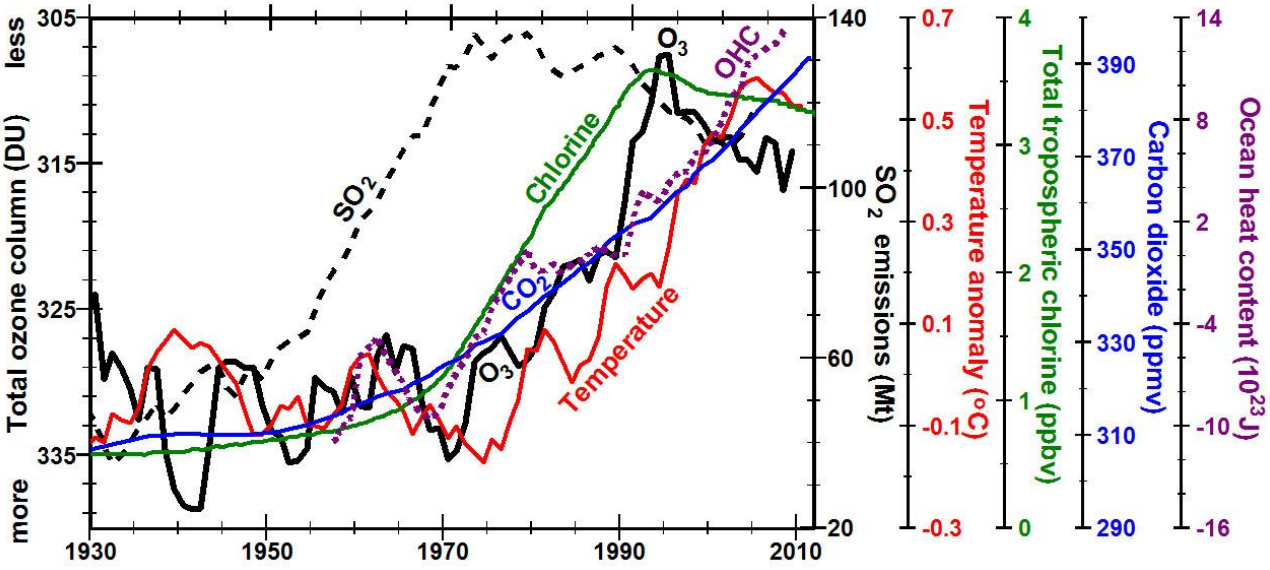

Fig 5. Increased SO_2 pollution (dashed black line) does not appear to contribute to substantial global warming (red line) until the total column ozone (black line, y-axis inverted) decreased, most likely due to increasing tropospheric chlorine (green line). Annual total column ozone at Arosa, Switzerland (*37*), mean annual temperature anomaly in the Northern Hemisphere in reference to the average from 1961-1990 (*12*), and ocean heat content (OHC) in reference to the average from 1955-2006 (dashed purple line) (*43*) are smoothed with a centered 5 point running mean.

World ocean heat content (dashed purple line) increased from 1970 to 1980, remained relatively constant until 1990, and has been increasing ever since (*43*). The time relationship between ocean heat content, volcanism, and annual total ozone is shown more clearly by the dashed red line in Figure 3 where the ozone data have not been smoothed. The slow change in

ocean heat content between 1980 and 1990, smoothed with a 5-year running mean, reflects the observed global cooling of up to 0.5°C for up to three years following the eruptions of El Chichón (1982) and Pinatubo (1991) (*85*). Continued rise of ocean heat content since 1998 is expected since column ozone has remained depleted.

SO_2 emissions (dashed black line), 88% from burning fossil fuels (*86*), rose rapidly from 1950 until 1973 when concern over acid rain led to the addition of smokestack-scrubbers and other technologies, primarily to electric generating and certain mineral processing facilities, as well as substitution of North Sea oil for coal in Europe. The result was a 20% decrease in SO_2 emissions by 2002. Similar increases were observed in NO_X, methane, and black carbon accompanied by a decrease and then increase in surface solar radiation (Figure S3).

The annual rate of increase in concentrations of CO_2 (blue line) (*87*) was <0.1 ppm/yr from 1938 to 1947 but began increasing to 0.7 ppm/yr by 1960 as concentrations of SO_2 and other anthropogenic pollutants (Figure S3) were rapidly increasing. From 1976, when ocean heat content began increasing, the annual rate of increase of CO_2 doubled and even quadrupled to between 1.3 and 2.7 ppm/yr most likely due to decreasing CO_2 solubility in a warming ocean. Annual CO_2 concentrations increased with industrialization and with ocean temperature, but slowed during the three years following major volcanic eruptions even though CO_2 was the second most voluminous gas erupted after water vapor.

SO_2 and related pollution increased ~30 years before the major increase in temperature suggesting that major increases in anthropogenic pollution did not affect global temperatures until ozone was depleted, allowing ultraviolet radiation with energy high enough to cause photodissociation into the lower troposphere. Thus absorption without photodissociation does not appear to cause substantial global warming. Similarly, the observation that the lowest temperatures in the stratosphere are near the base of the ozone layer where ozone concentrations are highest implies that simple absorption by ozone is less important for warming the stratosphere than absorption that leads to photodissociation.

Absorption by greenhouse gases: But what about the effects of absorption of infrared radiation by greenhouse gases such as water vapor, carbon dioxide, and methane? Since 1998, concentrations of CO_2 increased monotonically at an accelerating rate, while mean global temperatures remained relatively constant (*82, 88*). The sensitivity of climate to a doubling of carbon dioxide has not been observed directly in nature nor in the laboratory; it has been estimated by assuming temperature increases in the past 50 years, at the end of ice ages, or during periods of major warming millions of years ago resulted primarily from absorption by greenhouse gases. Yet photodissociation and ozone depletion clearly contribute to warming and can explain the location and timing of regional warming much more directly than greenhouse gases distributed relatively homogeneously around the globe.

There are several issues explained in more detail in the SOM that need to be evaluated before we can determine quantitatively the relative importance of greenhouse gases:

1. Molecules of greenhouse gases are well documented to absorb radiant energy along spectral lines that correspond to combinations of the resonant frequencies of the gas molecule's chemical bonds and rotational degrees of freedom (Figures S1 and S2) (*19*). This means that oscillatory kinetic energy in the radiation field is absorbed as oscillatory kinetic energy within each molecule. But temperature of a gas is proportional to translational kinetic energy. What proportion of the oscillatory kinetic energy is

converted to translational kinetic energy during the numerous collisions of gas molecules in the atmosphere?

2. An incandescent light bulb emits a broad spectrum of radiation described by Planck's law for black-body radiation (blue line, Figure S1) and is perceived as being hot. A fluorescent light bulb emits radiation over very narrow parts of the visible spectrum (black line, Figure S1) and is perceived as being cool. Over how broad a spectrum does a layer of molecules dispersed in a gas radiate? Is a layer of gas properly described as a black body? Does such a layer ever reach local thermodynamic equilibrium?
3. Heat in matter flows from warm to cool. If radiation is absorbed via resonance, which it appears to be, heat flows from higher spectral intensity in the radiation field to lower spectral intensity within the molecule. While radiation propagates in all directions, absorption may only occur from higher to lower spectral amplitude; otherwise the radiation is reflected. Can radiation from an atmospheric layer that is cooler than Earth be absorbed by Earth? Radiation from Earth probably reaches the Sun (Figure S1), but that does not mean it is absorbed by the Sun; it is most likely reflected. Our bodies absorb radiant heat, but we do not perceptively absorb radiant cold; instead we lose body heat more efficiently into a cold environment. We sense an ice cube by touch and the flow of heat from our body to the ice cube.

Each of these issues will need to be examined in detail in the laboratory and in nature before we can calculate the relative importance of absorption by greenhouse gases compared to photodissociation enhanced in the troposphere by depletion of total column ozone.

High-resolution paleoclimatic studies in the Late Miocene (*89*) and the existence of glaciation in Devonian and Permian-Triassic times when CO_2 concentrations were >10 and >5 times preindustrial values respectively (*90*) question a strong coupling between CO_2 concentrations and oceanic warmth. Similarly the width of the tropical belt widened 2^o to 5^o in latitude since 1979 (*91*). While expansion in the Southern Hemisphere has been attributed to ozone depletion (*92, 93*), Allen et al. (*94*), use the Community Atmosphere Model version 3 to suggest that "recent Northern Hemisphere tropical expansion is driven mainly by black carbon and tropospheric ozone, with greenhouse gases playing a smaller part." Black carbon absorbs strongly at visible wavelengths and even more in the ultraviolet (*95, 96*).

Periods of sudden global warming are contemporaneous with major increases in volcanism at the end of the last ice age (Figure S4), during 13 Dansgaard-Oeschger sudden warming events in the past 46,000 years, during the opening of the North Atlantic in the Early Eocene, and during the 12 largest mass extinctions over the past 360 million years (*97*) explained in more detail in the SOM.

Modeling: So far, we have reviewed observations showing that photodissociation of O_2 and O_3 warms the stratosphere, that depletion of total column ozone moves this warming down into the troposphere cooling the lower stratosphere, that the lower stratosphere cooled more than 2^oC since 1957, that mean surface temperatures in the Northern Hemisphere increased ~0.8^oC during the same time period as stratospheric cooling, that stratospheric cooling occurred primarily in steps following the times of major volcanic eruptions, and that the greatest regional increases in surface temperatures occurred at the times and locations of the greatest depletion of ozone. Modeling these observed changes accurately will require understanding at least:

1. Seasonal and yearly timing and location of ozone depletion caused by all volcanic eruptions, ongoing volcanic emissions, and anthropogenic chlorofluorocarbons
2. Effects of ozone depletion on transmission of ultraviolet energy through the atmosphere

3. Efficiency of converting that radiation to temperature in a polluted atmosphere, in the ocean, and on land with varying albedo
4. Efficiency of radiation from land, water, ice, and snow at night
5. Effects of solar zenith angle not only on energy per square meter, but also on increasing the path length over which photodissociation can occur
6. Partitioning of energy absorbed in a polluted environment to warm the air versus energy absorbed directly by land and by ocean to warm the climate system
7. Efficiency of transmission of ultraviolet radiation through clouds, water vapor, and water
8. Feedbacks such as the effects of a cooling stratosphere caused by ozone depletion on increasing that depletion

Conclusions: When total column ozone is depleted by chemically active forms of chlorine and bromine emitted by man and volcanic eruptions, more ultraviolet energy with wavelengths primarily between 290 and 340 nm penetrates into the troposphere. This energy can be absorbed in a polluted lower troposphere, causing warming by increased photodissociation of anthropogenic ozone and nitrogen dioxide. In a less polluted environment, most of this energy penetrates more than ten meters into the ocean, increasing ocean heat content far more effectively than infrared radiation absorbed near the surface where the energy is radiated back into the atmosphere each night. Absorption by any gas of radiant energy not energetic enough to cause photodissociation does not appear to cause substantial warming. Observed warming is greatest in mid to polar latitudes during winter where and when ozone depletion is greatest. Climate change on scales of years to billions of years appears controlled primarily by changes in the rates and volumes of volcanism: effusive basaltic eruptions primarily cause warming while andesite/dacitic explosive eruptions cause net cooling.

Acknowledgments: All data plotted in this paper are available on Internet at locations referenced in the text. Thanks to Johannes Staehelin and Rene Stuebi for updates to the ozone data from Arosa and to Vidali Fioletov for access to preliminary ozone data from Toronto.

Critical comments by Huiming Bao, James Bjorken, Terrance Gerlach, Peter Giles, Zach Hall, William Happer, Bertram Raynes, and Adrienne Ward helped me to be more precise. Special thanks to Michael MacCracken and Peter Molnar who questioned my interpretations through thoughtful reviews of the six quite different total rewrites of this paper over several years. I greatly appreciate the hard work by the many contributors to Wikipedia who provide an important first step for understanding the many fields of science researched to produce this paper and Google Scholar for providing instant access to the details.

Supplementary Materials:

www.sciencemag.org

Text

Figures S1-S6

References (98-158)

Supplementary Materials

Temperature versus absorption spectra: According to Planck's law, a black body, an idealized perfect absorber and emitter of electromagnetic radiation, radiates the spectral intensity shown by the solid lines in Figure S1 assuming 5770K as the temperature for Sun and 288K for Earth. The shapes of these lines are similar, but the wavelength of maximum spectral intensity (λ_{max}) decreases with increasing temperature according to Wien's displacement law where λ_{max} in micrometers (μm)(1 μm=1000 nm) equals 2897 divided by temperature in Kelvin or the color temperature max (T_{max}) of EMR at λ_{max} equals 2897 divided by λ_{max}. Since radiation diverges with distance, the dashed red line shows the radiation from the sun at the top of Earth's atmosphere.

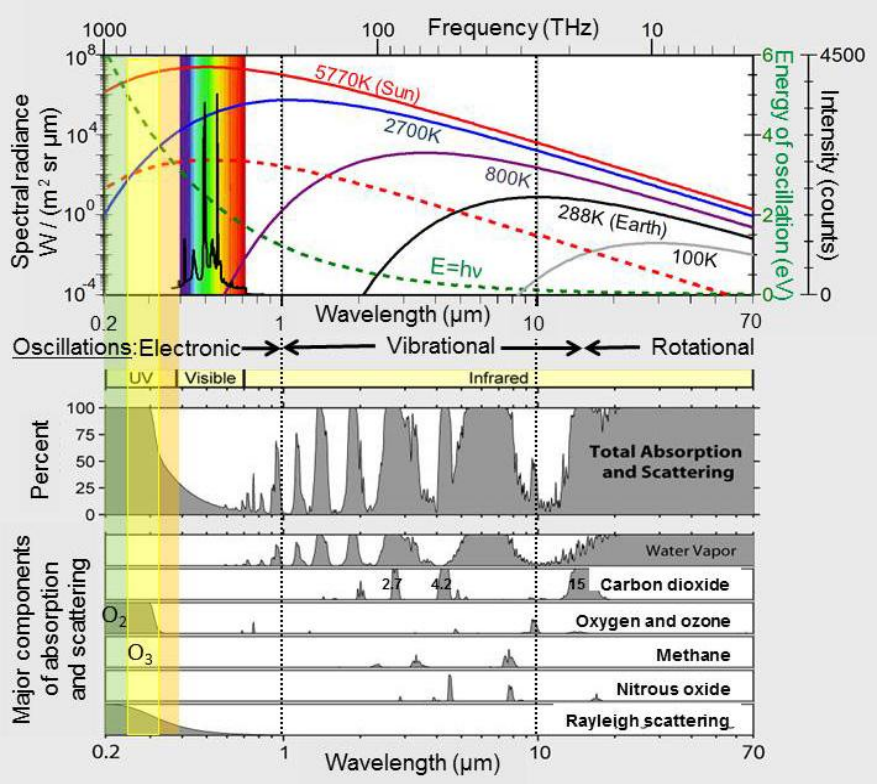

Fig. S1. The spectral radiance from a black body such as an incandescent light bulb (blue line, 2700K) is over a broad spectrum, while the radiance from a fluorescent light bulb (black line on top of the rainbow of visible light) is confined to very narrow parts of the visible spectrum. The incandescent light bulb has perceptible heat, the fluorescent bulb does not. Absorption by greenhouse gases shown in the lower part is also confined to very narrow spectral bands (*98*).

The blue curve shows the spectrum radiated by a typical incandescent light bulb where the temperature of the tungsten filament is 2700K thermally isolated from the bulb by a partial vacuum. Note how little of the energy radiated is in the visible spectrum (rainbow colors from violet to red, 0.380-0.750 μm). Most energy is in the infrared and this is what we perceive as temperature (heat). The radiation from a typical fluorescent lamp with rare-earth phosphor is shown by the black line overlying the visible spectrum (*80*). The y-scale for intensity is not scaled to the spectral radiance. Ultraviolet light generated inside the lamp tube causes the terbium, mercury, and europium coating on the glass tube to fluoresce especially strongly at 0.5424, 0.5465 and 0.6116 μm respectively emitting almost all the radiation within the visible

spectral band accompanied by very little heat. This is why fluorescent bulbs produce much more visible light using much less energy than incandescent bulbs and why they do not get as hot. The three spectral peaks have color temperatures of 5341K, 5301K, and 4737K respectively but this is really not temperature as we perceive it. We can think of it as microscopic color temperature representing the frequency of the microscopic oscillation of the terbium, mercury, and europium molecules, but there is no warmth without the broad spectrum of infrared radiation.

Greenhouse gases similarly absorb narrow spectral ranges of radiation from Earth and Sun shown in the lower half of Figure S1. The details of the 15 μm peak for carbon dioxide are shown in Figure S2. Each spectral line has a finite width normally assumed to be a Lorentz line shape. The energy associated with the line is Planck's constant (h) times the frequency (ν) times the area under the line, or more precisely the integral of hν times the spectral intensity as a function of frequency over the Lorentz line shape. This is a very small amount of thermal energy. The oscillatory energy in the radiation field is absorbed by increasing the oscillatory energy of each of the normal modes of oscillation for each of the degrees of freedom and various combinations of different degrees of freedom of each absorbing molecule. This oscillatory energy in gas molecules is not perceptible as heat (temperature) until it is converted into translational kinetic energy averaged among all the other gas molecules by the billions of collisions per second that occur in gases near Earth's surface. The efficiency of this conversion is not clear, but by the classical law of equipartition, only some oscillatory energy would be converted. The total amount of energy involved is small compared to the broadband radiation spectrum from Earth.

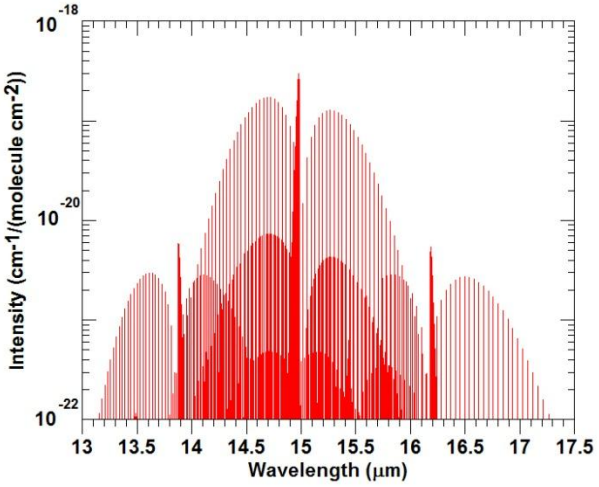

Fig. S2. Absorption of infrared electromagnetic radiation by CO_2 is very selective along spectral lines.

The very narrow spectral lines of absorption imply high-Q resonance such that the oscillatory electromagnetic energy transferred from the field to the molecule at each resonant frequency is equal to one-half the difference between the intensity (spectral radiance) in the field at the resonant frequency and the intensity in the molecule at the same frequency. This means that oscillatory energy (microscopic heat) only flows from higher intensity to lower intensity so as to equalize intensities. When substantial mass "bakes" in sunlight, such as a rock in the desert, the shorter wavelength, higher microscopic color temperature energy must be absorbed by the rock but then heat flows within the rock to raise the temperature of the rock over a wide spectrum such as plotted in Figure S1. Thus It does not seem appropriate to assume, as most

radiation codes do, that radiation from layers in the atmosphere that are cooler than Earth's surface is absorbed at Earth's surface. Radiation from earth may propagate to the sun, but that does not mean it is absorbed by the sun; it is most likely reflected.

The green shaded band in Figure S1 shows wavelengths less than 0.242 μm that dissociate molecular oxygen (O_2). The yellow band shows wavelengths between 0.242 μm and 0.310 μm that dissociate ozone (O_3). The orange band shows wavelengths between 0.310 μm and visible light (0.380 μm) that can dissociate O_3 and NO_2 at lower quantum yield. The dashed green line shows Planck's postulate (E=hν). Note how the energy of solar radiation absorbed by a molecule of ozone at a wavelength of 0.310 μm (4.3 eV) is 52 times greater than the energy at 15.0 μm (0.0827 eV) absorbed by a molecule of CO_2 and that all of the energy absorbed to sever the O_3 molecular bond is converted by photodissociation directly into translational kinetic energy (temperature of a gas) while only a fraction of the energy absorbed by CO_2 is converted to temperature through collisions.

Relative timing of pollution: Related to Figure S3 and Figure 5 in the main paper, note:

1. Mean surface temperatures (red line) (*12*) increased during the 1930s, cooled during the 1940s, remained relatively constant until 1975, rose rapidly until 1998, and remained relatively constant since. The temperature increase was 30% greater in the northern hemisphere containing 90% of human population and most of the anthropogenic pollution.
2. SO_2 emissions (black line) (*86*), 88% from burning fossil fuels (*99*), rose rapidly until 1973, when concern over acid rain led to the addition of smokestack-scrubbers and other technologies, primarily to electric generating and certain mineral processing facilities, as well as substitution of North Sea oil for coal in Europe. The result was a 20% decrease in SO_2 emissions by 2002. But rapid growth in Asia of industry and particularly electric power generation caused global SO_2 emissions to begin increasing again in 2002.
3. Tree ring density and thickness normally increase with temperature, but since the 1940s these measures have diverged in northern forests (*100*). SO_2 is well-known to stress and even kill trees (*101, 102*). When anthropogenic SO_2 levels began to decline in the early 1980s, wide-spread greening in northern regions was observed from satellites (*103*).
4. NO_X emissions (olive line), 58% from vehicles and 34% from fossil fuels (*99*), shows a similar trend as SO_2 but with a slower decrease in vehicle pollution.
5. Black carbon emissions (dashed black line) (*104*), the product of incomplete combustion, began increasing at rates similar to SO_2, dropped precipitously with improvements in diesel-engine design, first applied in this accounting in 1965 (*105*), and leveled off by 2000 as emissions decreased in the West but increased in Asia.
6. Methane concentrations (green line) (*106-108*) increased gradually with emissions of other pollutants, reached a relatively constant rate of increase of ~14 ppb/year from 1955 to 1992, stopped increasing by 2006 and began increasing again at a rate of ~6 ppb/year in 2007 (*106, 107*). The lifetime of methane is ~12 years, much longer than any of the ultraviolet-energy-absorbing pollutants, partially explaining the time lag. Methane concentrations are increased by fossil fuel use (*109*), biomass burning, certain types of agriculture (*110*), and thawing of permafrost. Methane is removed from the atmosphere when oxidized by OH. Changes in OH available may explain much of the observed changes in methane.

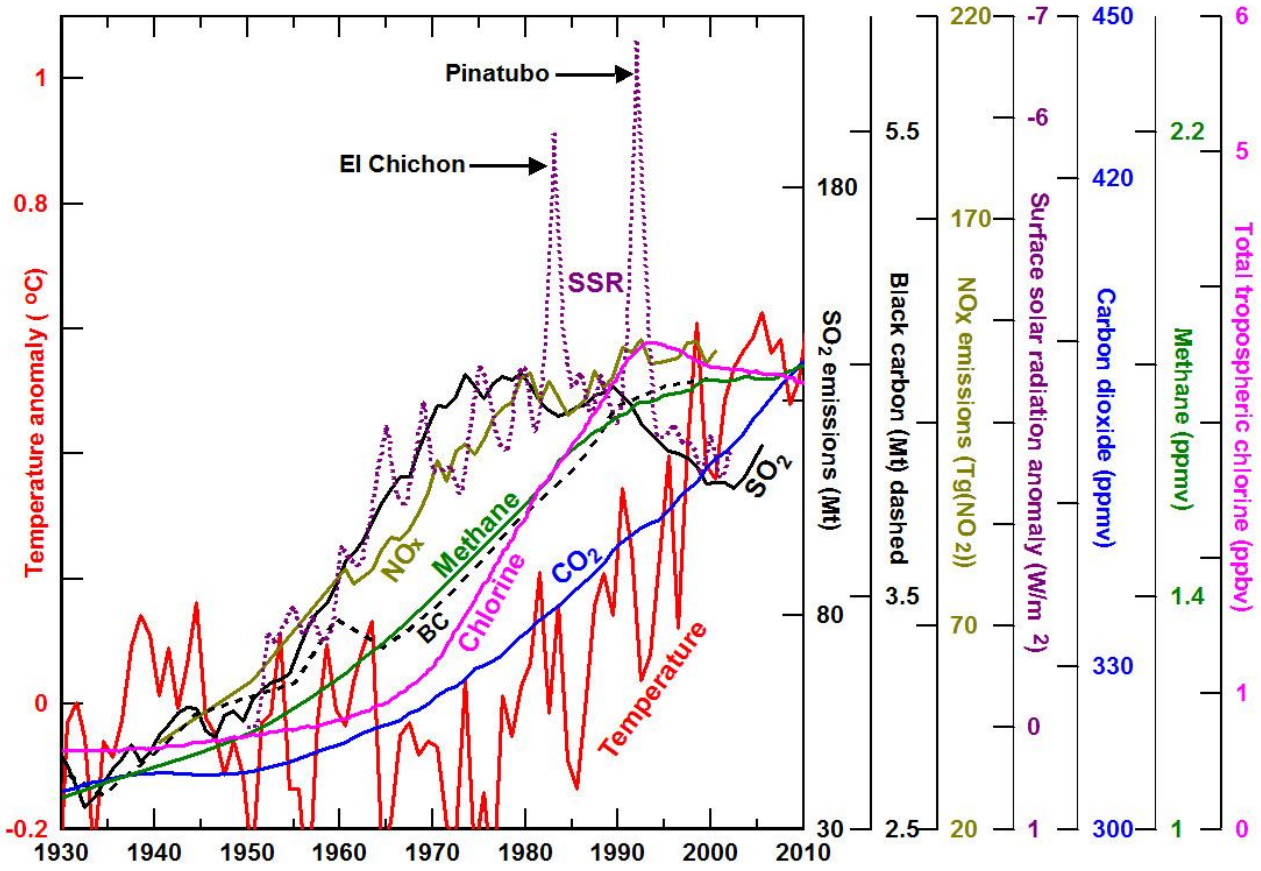

Fig. S3. Increases in temperature and methane concentrations and decreases in surface solar radiation (SSR) reflect increases in pollution (SO_2, NO_X, and black carbon), not the constant rise in CO_2 concentrations. NO_x data from RETRO (*111*) interpolated before 1960 from US data (*112*) are thought to be constant or slightly decreasing since 2000 (*113*).

7. OH concentrations increase with increasing NO_X, tropospheric O_3, and sunlight, and decrease with increasing SO_2, CO, methane, and other pollutants it oxidizes. Global concentrations of OH are difficult to observe and model and are affected by many factors, but modeling suggests they have decreased 9% since preindustrial times (*114*). CH_2O data from Greenland suggest OH concentrations may have decreased by as much as 30% (*115*). Detailed observations show a gradual decrease from 1980 to 2000 (*116*).
8. CO in the northern hemisphere increased 0.85%/year from 1950 to 1987 (*117*), decreased very slightly from 1988 (when detailed measurements began) to 2001, and increased slightly to 2005 (*118*).
9. Concentrations of water vapor and ozone in the lowermost stratosphere increased until 2000 but began decreasing suddenly in 2001 (*119, 120*) when emissions of SO_2 stopped declining and began to increase again.
10. Total tropospheric chlorine caused by anthropogenic chlorofluorocarbons (fuchsia line) increased rapidly after 1970 but reached a peak in 1993 due to implementation of the Montreal Protocol and is expected to return to late-1970s levels by 2040 (*42*).
11. Annual total column ozone at Arosa, Switzerland (green line, y-axis reversed, Figure 5), fell rapidly from 1970 to 1994 as a result of the rise in chlorine, and has been increasing ever since (*37*).

12. The purple dotted line (y-axis reversed) shows simulated annual clear-sky surface solar radiation (SSR) anomalies for mid-latitudes in the northern hemisphere (*121*). SSR decreased with increasing SO_2 and related pollution and increased with decreasing pollution. SSR decreased rapidly in East Asia after 2000 in phase with dramatic local increases in SO_2 and BC emissions (*122*). Note the rapid decreases in SSR for ~3 years following the large volcanic eruptions of El Chichón and Pinatubo.
13. Yearly CO_2 concentrations rose monotonically (blue line, Figures 5 and S3) (*123, 124*). Climate models that assume CO_2 is the primary driver of temperature increase have overestimated global warming since 1998 (*125, 126*) and are probably overestimating warming in future decades.

Increases in all these types of pollution did not raise global temperatures until chlorine (fuchsia line) increased, depleting total column ozone (green line, Figure 5).

Volcanism is a primary driver of climate change: Layers of ice beneath Summit Greenland that contain the largest concentrations of volcanic sulfate per century (red line, Figure S4) (*127*) also contain $\delta^{18}O$ evidence (*128*) for the most rapid global warming (green line) during the Bolling warming (B), decreasing during the cooler Younger Dryas (Y), and increasing again during the Preboreal warming (P). Volcanic sulfate is total sulfate minus the small contributions from sea salt and dust based on sodium and calcium content (*129*). Volcanic sulfate forms through oxidation of SO_2 emitted by volcanoes. The rapid increase in "volcanic" sulfate during the 20^{th} century primarily results from anthropogenic emissions of SO_2 (Figures 5 and S3) from northern Russia, northern Europe, and central North America (*130*).

This temporal association of SO_2 emissions with warming over the past 25,000 years is unambiguous. Sulfate and the $\delta^{18}O$ proxy for temperature are measured in the same ice layers so there is little error in relative timing. Peak sulfate per century during peak warming (2028 ppb) is 218 times greater than average sulfate per century (9.3 ppb) during the last glacial maximum (LGM, Figure S4) (21-25 thousand years before present) and 441 times greater than average sulfate (4.6 ppb) between 5 and 1 thousand years before present. 63% of the 7000 ice layers measured contain zero sulfate. Yet nearly all large explosive volcanic eruptions observed throughout written history caused cooling of ~0.5^oC for up to 3 years. How can volcanoes be associated with both cooling and warming?

This enigma has driven my research since 2006. In 2009, I published a paper (*97*) documenting the association of volcanism with global warming, global cooling, mass extinctions, and drought and proposed that the differences were due to different rates of volcanism and the chemical effects of SO_2. More recent research described in this paper shows that SO_2 does not cause warming directly (Figure 5) but that oxidized SO_2 (sulfate) is the footprint of the level of volcanic activity recorded in glacial ice and that the enigma is explained by the balance of ozone depletion versus stratospheric aerosols. Hegerl et al. (*131*) similarly found that detailed reconstructions of global temperature over the past 1500 years suggest that "natural forcing, particularly by volcanism, explains a substantial fraction of decadal variance." What are the details of these mechanisms?

Volcanoes erupting andesitic, dacitic and other evolved magmas typically eject 5 to 25 Mt SO_2 into the lower stratosphere where it is oxidized by OH to form sulfuric acid with an e-folding time of ~35 days (*132*) but up to 13 months in the Arctic (*133*). Sulfuric acid has a very

low vapor pressure, aggregating rapidly on particles. Growth of these particles is enhanced in the non-turbulent stratosphere where solar and chemical warming leads to continued lofting and

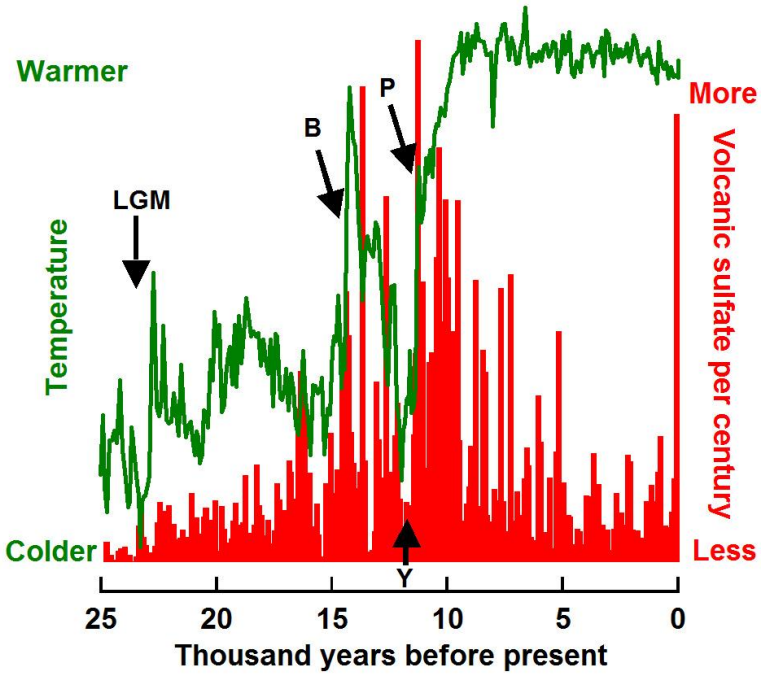

settling evidenced by the very low thermal gradient in the lowermost stratosphere (Figure 1).

Fig. S4. Volcanic sulfate per century (red) is unusually high during periods of rapid warming (green), suggesting volcanism is contemporaneous with global warming. Volcanic sulfate ranges from 0 to 2028 ppb. "Volcanic" sulfate in the 20th century is cause primarily by anthropogenic emissions. The value shown (1910 ppb) is twice the sum observed during the 50 years from 1935 through 1984. The increase in equatorial Pacific sea surface temperature since the last glacial maximum (LGM) is on the order of 2.8°C (*134*).

Several months after the eruption of Pinatubo in 1991, particle sizes were typically 300 to 500 nm, reflecting, Mie scattering, and absorbing sunlight, warming the stratosphere 2-3°C within 4-5 months (purple line, Figure 3), and cooling Earth up to 0.5°C for three years (*135*). These stratospheric aerosols decreased average total solar irradiance at Earth's surface by less than 1% (*136*). Modeling shows that such cooling may have affected ocean temperatures for more than 100 years following the VEI=6 eruption of Krakatoa in 1883 (*137*) and that cooling can accumulate over many eruptions (*138*) incrementing the globe into an ice age when rates of major explosive volcanism are 5 to 10 times more active than throughout written history (*97*). SO_2 is widely assumed to have the same cooling effect in the troposphere, but this seems highly unlikely. With an e-folding time of 35 days to be oxidized, SO_2 is spread around the world and replenished continuously by anthropogenic emissions (*139, 140*). Furthermore the particle sizes cannot grow large enough to reflect significant amounts of sunlight due to turbulence except possibly by circulation in certain types of clouds.

These large volcanic eruptions also deplete total column ozone for up to a decade, but the absorption, reflection and scattering of sunlight by the aerosols is more dominant for the first few years except during northern winters where and when ozone depletion is greatest. Temperatures over large parts of continents in the northern hemisphere, increase by as much as 3°C during the two winters following the 1991 eruption of Pinatubo (*53*).

Volcanoes on oceanic islands such as Iceland and Hawaii, erupt more primitive basaltic magmas, extrude cubic kilometers of lava flows on the surface, display impressive lava fountains often along kilometers of linear vents, emit megatons of SO_2 and halogens such as chlorine, bromine, and fluorine, but rarely eject these gases into the stratosphere. Global warming predominates because ozone depletion is substantial and cooling by aerosols is minimal.

Warming was clearly observed during the ten eruptive phases of the fissure volcano Laki (Lakagigar) in South Iceland from June 8, 1783 until February 7, 1784 (*141*), the largest basaltic lava flow in written history except for the eruption of nearby Eldgjá in 934 A.D. Laki ejected ~24 Mt of SO_2 into the lower stratosphere where it most likely spread eastward and northward ultimately providing cooling. Pinatubo only erupted ~17 Mt SO_2, but Laki ejected an additional ~96 Mt SO_2 into the troposphere where the jet stream carried much of it southeastward to Europe. Severe acid damage to vegetation from Iceland to Eastern Europe, to Italy suggests concentrations of SO_2 could have been as high as 1,000 ppb (*141*), roughly three orders of magnitude larger than background. A "dry fog" blanketed much of Europe primarily from June 14 through August. "Many people experienced troublesome headaches, respiratory difficulties, and asthma attacks"(*141*). SO_2 is invisible but when absorbing ultraviolet radiation, the electronic transitions cause fluorescence in the visible spectrum explaining this "dry fog". In July, surface temperatures increased as much as 3.3^{o}C above the 30-year mean centered on 1783, the highest temperatures recorded from the first measurements in 1659 until 1983 (*141, 142*). There was not time for significant amounts of aerosol to form in the stratosphere nor for ozone to be depleted by chlorine released through heterogeneous processes. But the eruption did release ~7 Mt of hydrochloric acid and ~15 Mt of hydrofluoric acid (*143*) that could have caused rapid depletion of ozone.

The Laki eruption deposited ~115 ppb sulfate in snow at Summit Greenland (*127*). During the major Preboreal warming (P in Figure S4) (11,700-9,800 years before present), sulfate per century in this ice was as much as 2028 ppb per century, 18 times more than from Laki. Laki-type activity continuing for these 1900 years appears to have played a major role in finally warming the oceans out of the last ice age. Basaltic volcanism under ice leads to long, flat-topped, steep-sided table mountains or tuyas found throughout Iceland. "12 of the 13 dated table mountains experienced their final eruptive phase during the last deglaciation" (*144*).

Volcanism was similarly highest during the other 13 Dansgaard-Oeschger sudden warmings between 46,000 and 11,600 years before present when tropical sea-surface temperatures rose ~3^{o}C in a decade or two and then decreased back to ice-age temperatures over decades to centuries as volcanism waned before the deep ocean could be warmed (*97, 145, 146*).

The Late Paleocene thermal maximum (54.18-53.90 Ma, million years before present) is contemporaneous with the massive sub-aerial volcanism during the opening of the North Atlantic Ocean (*147*).

Laki extruded 12.3 km^3 of lava flowing over an area of 565 km^2. Every 25 million years, on average, there have been massive eruptions of millions of cubic kilometers of basalt typically associated with major mass extinctions (*97, 148, 149*). The Siberian Traps, for example, extruded ~250 Ma, cover an area today larger than the states of Washington, Oregon, California, Idaho, Nevada, and Arizona combined and when forming may have covered an area as large as 71% of the size of the United States (*150*). Visscher et al. (*151*) document increased mutations in

herbaceous lycopsids during the end-Permian mass extinction that imply substantial depletion of ozone.

The location, volume, type, and timing of volcanism are determined by the motion of large lithospheric plates (plate tectonics). Sub-aerial basaltic eruptions are most common on islands along mid-ocean ridges and places where these ridges are overrun by continents. Major explosive volcanoes are most common where oceanic plates are being subducted beneath continents, such as around most of the Pacific Ocean. Explosive eruptions generally cool Earth, incrementing it into an ice age if sufficiently frequent; basaltic eruptions general warm Earth (*97*). Basaltic eruptions deep under oceans do not appear to influence climate directly, but major increases in the area of ocean crust formed per year at 33.9, 12, and 3 Ma, implying major increases in rates of subduction, are associated with major cooling (*97, 152*). Sulfate and ash in ice cores record the level of volcanism faithfully, but the ratio of stratospheric aerosols to ozone depletion controls the effects of this volcanism on temperature.

Apparent increase in ozone during years with large volcanic eruptions: Total annual column ozone observed at Arosa appears to have increased 12 DU (3.9%) in 1991 when Pinatubo erupted 10,300 km to the southeast but decreased 28 DU (8.5%) by 1993 (Figure 3). Similarly ozone appears to have increased 14 DU (4.4%) in 2010 when Eyjafjallajökull erupted, only 2600 km to the northwest, but decreased 28 DU (8.4%) in 2011. Other volcanic eruptions shown in Figure 3 are also contemporaneous with a modest increase followed the next year by a much larger decrease.

The apparent ozone increase in 2010 occurred primarily between February 19 and February 26, ~4 weeks before the first effusive flank eruption of basalt from March 20 to April 12 and ~7 weeks before the main explosive eruption of trachyandesite on April 14. Figure S5 shows that total ozone northeast of Iceland increased to more than 550 DU on February 19 over a background of ~325 DU, an increase of ~70%. The deviation of total ozone over the period from February 21 to February 28 increased 45% compared to mean levels from 1978 thru 1988 (Figure S6) (*76*).

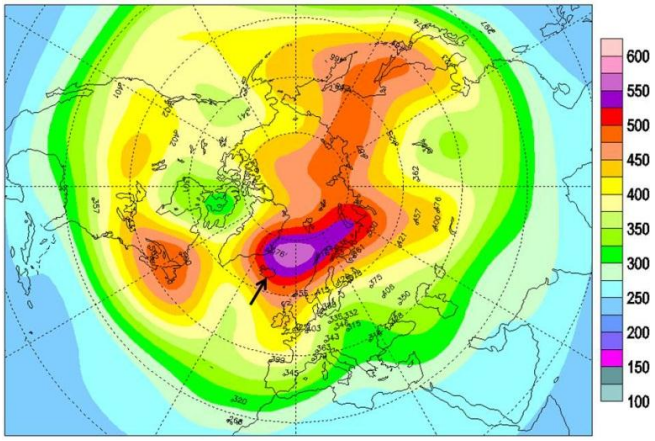

Fig. S5. A total "ozone" anomaly >550 DU was observed northeast of Iceland (black arrow) on February 19, 2010, based on the satellite borne Total Ozone Mapping Spectrometer (TOMS) integrated with data from ground stations (*76*).

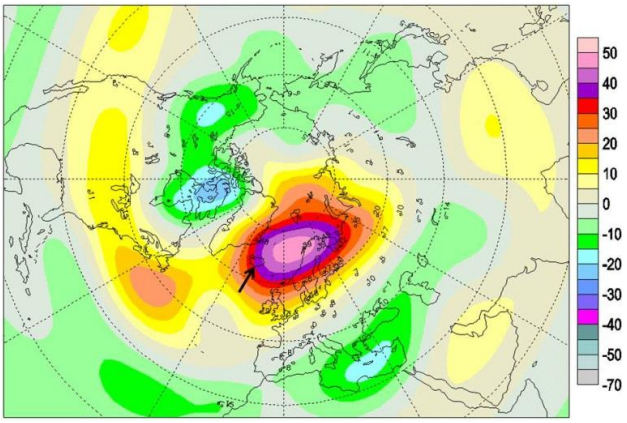

Fig. S6. The deviation of total ozone observed northeast of Iceland (black arrow) from February 20 through 28, 1991, from the mean of 1978-1988 levels was as high as 50% (*76*).

At Eyjafjallajökull, seismic activity and deformation began in December, 2009, "explained by a single horizontal sill inflating at a depth of 4.0-5.9 km under the southeastern flank of the volcano" (*153*). Deformation increased exponentially in February, suggesting a major change in pressure conditions within the system by March 4. Thus a substantial release of gas from the top of the magma body is highly likely to have occurred in late February as the roof of the intrusion fractured to the surface.

Ozone is not a likely volcanic gas because magma has a reduced oxidation state at high temperature. Primary gases observed from high-temperature fumaroles include sulfur dioxide, which absorbs ultraviolet solar radiation strongly at the same wavelengths as ozone (Figure 2) and is known to affect ozone measurements in urban areas such as Uccle, just outside of Brussels, Belgium (*154*). Basaltic effusive eruptions typically emit 10 to 100 times more sulfur dioxide per cubic kilometer of magma than the more explosive eruptions from volcanoes such as Pinatubo with more evolved magmas (*70-72*). Sulfur dioxide is colorless so that its release from high-temperature fumaroles in the vicinity of the effusive eruption that began on March 20 would have gone unnoticed if substantial water vapor was not included. There were no instruments in the vicinity to detect it.

Another possibility is that high-temperature gases from basaltic magma (1300-1400^{o}C) (*155*) may interact in some way with water released from the magma, with ground water, or even with atmospheric water vapor to form oxygen atoms and thus ozone. Magmatic high-temperature gases might also interact with volatile organic compounds or nitrogen compounds or gases to form ozone catalytically.

Local farmers noted unusual melting of snow near high temperature fumaroles "months" before the eruption of Hekla in south Iceland on May 5, 1970 (*156, 157*).

Mt. Pinatubo in the Philippines (120^{o}E) showed signs of reawakening with a group of felt earthquakes on March 15, 1991, the first steam explosions on April 2, first eruption on June 12, and the main eruption on June 15. Ozone anomalies >525 DU occurred from late January, 1991, through April 25, primarily at latitudes >50^{o}N. The Brewer-Dobson circulation is thought to move ozone and related gases from the latitude of Pinatubo (15^{o}N) up into the stratosphere, northward, and then downward north of 50^{o}N (*158*). The spatial and temporal correlations are not as clear as for Eyjafjallajökull because while Pinatubo was a much larger explosive eruption,

the changes in the magmatic plumbing system are not as well-known and the magma was not basaltic.

Maps of total ozone such as in Figure S5 are produced daily and could prove useful in determining when intruding magmas begin to release gases to the surface, especially for basaltic magmas, but extensive work is still needed to map the nature of these large apparent ozone anomalies and to understand their chemistry.

References and Notes:

1. R. J. Reed, The role of vertical motion in ozone-weather relationship. *J. Meteorol.* **7**, 263 (1950).
2. V. Fioletov, Ozone climatology, trends, and substances that control ozone. *Atmos. Ocean* **46**, 39 (2008).
3. Committee on Extension to the Standard Atmosphere, *U.S. Standard Atmosphere, 1976* (U.S. Government Printing Office, Washington, D.C., 1976), pp. 241.
4. A. J. Krueger, R. A. Minzner, A mid-latitude ozone model for the 1976 US standard atmosphere. *J. Geophys. Res.* **81**, 4477 (1976).
5. B. J. Finlayson-Pitts, J. N. Pitts, *Chemistry of the Upper and Lower Atmosphere: Theory, Experiments, and Applications* (Academic Press, San Diego, 1999), pp. 969.
6. Y. Matsumi *et al.*, Quantum yields for production of $O(^1D)$ in the ultraviolet photolysis of ozone: Recommendation based on evaluation of laboratory data. *J. Geophys. Res.* **104**, 2001JD000510 (2002).
7. S. P. Sander *et al.*, *Chemical Kinetics and Photochemical Data for Use in Atmospheric Studies Evaluation Number 15* (Jet Propulsion Laboratory, 2006), vol. 06-2.
8. H. Schmidt *et al.*, The HAMMONIA chemistry climate model: Sensitivity of the mesopause region to the 11-year solar cycle and CO_2 doubling. *J. Clim.* **19**, 3903 (2006).
9. D. Kinnison *et al.*, Sensitivity of chemical tracers to meteorological parameters in the MOZART-3 chemical transport model. *J. Geophys. Res* **112**, D20302 (2007).
10. M. J. Molina, F. S. Rowland, Stratospheric sink for chlorofluoromethanes: Chlorine catalysed destruction of ozone. *Nature* **249**, 810 (1974).
11. D. J. Seidel, W. J. Randel, Variability and trends in the global tropopause estimated from radiosonde data. *J. Geophys. Res.* **111**, D21101 (2006).
12. www.cru.uea.ac.uk/cru/data/temperature/hadcrut3nh.txt (2012)
13. B. J. Finlayson-Pitts, J. N. Pitts, Chemistry of the Upper and Lower Atmosphere: Theory, Experiments, and Applications. (Academic Press, San Diego, 1999), Tables 3.7, 3.15, 3.16, 3.17.
14. S. Madronich, in *The Role of the Stratosphere in Global Change*, M. L. Chanin, Ed. (Springer-Verlag, Berlin, 1993) vol. 8, NATO ASI Series I: Global Environmental Change,pp. 463-471.
15. K. E. Trenberth, J. T. Fasullo, J. Kiehl, Earth's Global Energy Budget. *Bull. Am. Meteorol. Soc.* **90**, 311 (2009).
16. M. Tedetti, R. Sempéré, Penetration of ultraviolet radiation in the marine environment. A review. *Photochemistry and Photobiology* **82**, 389 (2006).
17. E. De Fabo, F. Noonan, T. Fears, G. Merlino, Ultraviolet B but not ultraviolet A radiation initiates melanoma. *Cancer Res.* **64**, 6372 (2004).
18. en.wikipedia.org/wiki/Vitamin_d (2012)
19. L. S. Rothman *et al.*, The HITRAN 2008 molecular spectroscopic database. *J. Quant. Spectrosc. Radiat. Transfer* **110**, 533 (2009).

20. C. Hermans, A. C. Vandaele, S. Fally, Fourier transform measurements of SO_2 absorption cross sections:I. Temperature dependence in the 24000–29000cm−1 (345–420nm) region. *J. Quant. Spectrosc. Radiat. Transfer* **110**, 756 (2009).

21. A. C. Vandaele, C. Hermans, S. Fally, Fourier transform measurements of SO_2 absorption cross sections: II.Temperature dependence in the 29000–44000cm−1 (227–345nm) region. *J. Quant. Spectrosc. Radiat. Transfer* **110**, 2115 (2009).

22. C. K. Folland *et al.*, in *Climate Change 2001: The Scientific Basis. Contribution of Working Group I to the Third Assessment Report of the Intergovernmental Panel on Climate Change*, J. T. Houghton *et al.*, Eds. (Cambridge University Press, Cambridge, UK, 2001) pp. 881.

23. K. E. Trenberth *et al.*, in *Climate Change 2007: The Physical Science Basis. Contribution of Working Group I to the Fourth Assessment Report of the Intergovernmental Panel on Climate Change*, S. Solomon *et al.*, Eds. (Cambridge University Press, Cambridge, United Kingdom and New York, NY, USA, 2007) pp. 235-336.

24. G. L. Hughes, S. S. Rao, T. S. Rao, Statistical analysis and time-series models for minimum/maximum temperatures in the Antarctic Peninsula. *Proceedings of the Royal Society A: Mathematical, Physical and Engineering Science* **463**, 241 (2007).

25. D. G. Vaughan *et al.*, Recent rapid regional climate warming on the Antarctic Peninsula. *Clim. Change* **60**, 243 (2003).

26. R. Mulvaney *et al.*, Recent Antarctic Peninsula warming relative to Holocene climate and ice-shelf history. *Nature* **489**, 141 (2012).

27. M. P. Meredith, J. C. King, Rapid climate change in the ocean west of the Antarctic Peninsula during the second half of the 20th century. *Geophys. Res. Lett* **32**, L19604 (2005).

28. A. Clarke *et al.*, Climate change and the marine ecosystem of the western Antarctic Peninsula. *Philosophical Transactions of the Royal Society B: Biological Sciences* **362**, 149 (2007).

29. S. E. Stammerjohn, D. G. Martinson, R. C. Smith, R. A. Iannuzzi, Sea ice in the western Antarctic Peninsula region: Spatio-temporal variability from ecological and climate change perspectives. *Deep Sea Res. Part II* **55**, 2041 (2008).

30. X. Wang, C. S. Zender, Arctic and Antarctic diurnal and seasonal variations of snow albedo from multiyear Baseline Surface Radiation Network measurements. *J. Geophys. Res.* **116**, F03008 (2011).

31. G. L. Manney *et al.*, Unprecedented Arctic ozone loss in 2011. *Nature* **478**, 469 (2011).

32. R. Kwok, N. Untersteiner, The thinning of Arctic sea ice. *Physics Today* **64**, 36 (2011).

33. NSIDC nsidc.org/news/press/2012_seaiceminimum.html (2012)

34. E. Rignot, I. Velicogna, M. R. van den Broeke, A. Monaghan, J. Lenaerts, Acceleration of the contribution of the Greenland and Antarctic ice sheets to sea level rise. *Geophys. Res. Lett.* **38**, L05503 (2011).

35. A. S. Gardner *et al.*, Sharply increased mass loss from glaciers and ice caps in the Canadian Arctic Archipelago. *Nature* **473**, 357 (2011).

36. P. Lemke *et al.*, in *Climate Change 2007: The physical science basis*, S. Solomon *et al.*, Eds. (Cambridge University Press, 2007) pp. 337-383.

37. J. Staehelin *et al.*, Total ozone series at Arosa (Switzerland): Homogenization and data comparison. *J. Geophys. Res.* **103**, 5827 (1998).

38. ftp://iaclin2.ethz.ch/pub_read/maeder/totozone_arosa_yearly (2012)

39. A. Douglass et al., in Scientific Assessment of Ozone Depletion: 2010. (World Meteorological Organization Global Ozone Research and Monitoring Project - Report No. 52, 2011) Figure 2-2.

40. P. J. Crutzen, The influence of nitrogen oxides on the atmospheric ozone content. *Q. J. Roy. Meteorol. Soc.* **96**, 320 (1970).

41. J. C. Farman, B. G. Gardiner, J. D. Shanklin, Large losses of total O_3 in atmosphere reveal seasonal ClO_x/NO_x interaction. *Nature* **315**, 207 (1985).

42. S. Solomon, Stratospheric ozone depletion: A review of concepts and history. *Rev. Geophys.* **37**, doi:10.1029/1999RG900008 (1999).

43. S. Levitus *et al.*, World ocean heat content and thermosteric sea level change (0-2000 m), 1955-2010. *Geophys. Res. Lett.* **39**, in press (2012).

44. Hadley Centre www.metoffice.gov.uk/hadobs/hadat/images.html (2012)

45. Remote Sensing Systems www.remss.com/msu/msu_data_description.html (2012)

46. en.wikipedia.org/wiki/Nuclear_weapons_testing (2012)

47. www.esrl.noaa.gov/psd/enso/mei/ (2012)

48. T. Druitt, Emplacement of the 18 May 1980 lateral blast deposit ENE of Mount St. Helens, Washington. *Bull. Volcanol.* **54**, 554 (1992).

49. R. P. Turco, O. B. Toon, R. C. Whitten, P. Hamill, R. G. Keesee, The 1980 eruptions of Mount St. Helens-Physical and chemical processes in the stratospheric clouds. *J. Geophys. Res.* **88**, 5299 (1983).

50. J. Gleason *et al.*, Record low global ozone in 1992. *Science* **260**, 523 (1993).

51. J. K. Angell, Estimated impact of Agung, El Chichon and Pinatubo volcanic eruptions on global and regional total ozone after adjustment for the QBO. *Geophys. Res. Lett.* **24**, 647 (1997).

52. J. Kerr, D. Wardle, D. Tarasick, Record low ozone values over Canada in early 1993. *Geophys. Res. Lett.* **20**, 1979 (1993).

53. A. Robock, Pinatubo eruption: The climatic aftermath. *Science* **295**, 1242 (2002).

54. M. De Mazière *et al.*, Quantitative evaluation of the post–Mount Pinatubo NO2 reduction and recovery, based on 10 years of Fourier transform infrared and UV-visible spectroscopic measurements at Jungfraujoch. *J. Geophys. Res.* **103**, 10849 (1998).

55. P. Johnston, R. McKenzie, J. Keys, W. Matthews, Observations of depleted stratospheric NO2 following the Pinatubo volcanic eruption. *Geophys. Res. Lett.* **19**, 211 (1992).

56. M. Koike *et al.*, Impact of Pinatubo aerosols on the partitioning between NO_2 and HNO_3. *Geophys. Res. Lett.* **21**, 597 (1994).

57. C. P. Rinsland *et al.*, Heterogeneous conversion of N_2O_5 to HNO_3 in the post-Mount Pinatubo eruption stratosphere. *J. Geophys. Res.* **99**, 8213 (1994).

58. M. T. Coffey, Observations of the impact of volcanic activity on stratospheric chemistry. *J. Geophys. Res.* **101**, 6767 (1996).

59. D. W. J. Thompson, S. Solomon, Understanding recent stratospheric climate change. *J. Clim.* **22**, 1934 (2009).

60. W. J. Randel, in *The Stratosphere: Dynamics, Transport and Chemistry, Geophysical Monograph Series*. (AGU, 2010) vol. 190,pp. 123-135.

61. J. K. Angell, Stratospheric warming due to Agung, El Chichón, and Pinatubo taking into account the quasi-biennial oscillation. *J. Geophys. Res.* **102**, 9479 (1997).

62. G. Brasseur, C. Granier, Mount Pinatubo aerosols, chlorofluorocarbons, and ozone depletion. *Science* **257**, 1239 (1992).

63. D. J. Hofmann *et al.*, Ozone loss in the lower stratosphere over the United States in 1992–1993: Evidence for heterogeneous chemistry on the Pinatubo aerosol. *Geophys. Res. Lett.* **21**, 65 (1994).

64. A. Ravishankara, Water vapor in the lower stratosphere. *Science* **337**, 809 (2012).

65. J. G. Anderson, D. M. Wilmouth, J. B. Smith, D. S. Sayres, UV Dosage Levels in Summer: Increased Risk of Ozone Loss from Convectively Injected Water Vapor. *Science*, 835 (2012).

66. Stratospheric Processes and Their Role in Climate: The Role of Halogen Chemistry in Polar Stratospheric Ozone Depletion www.atmosp.physics.utoronto.ca/SPARC/HalogenChem_Final_20090213.pdf (2009)

67. R. Salawitch *et al.*, Sensitivity of Ozone to Bromine in the Lower Stratosphere. *Geophys. Res. Lett.* **32**, L05811 (2005).

68. A. Vance *et al.*, Ozone depletion in tropospheric volcanic plumes. *Geophys. Res. Lett.* **37**, (2010).

69. A. Tabazadeh, R. P. Turco, Stratospheric chlorine injection by volcanic eruptions: HCI scavenging and implications for ozone. *Science* **260**, 1082 (1993).

70. J. Palais, H. Sigurdsson, in *Understanding Climate Change*, A. Berger, R. E. Dickinson, J. W. Kidson, Eds. (American Geophysical Union Geophysical Monograph, 1989) vol. 52,pp. 31-56.

71. C. Freda, D. Baker, P. Scarlato, Sulfur diffusion in basaltic melts. *Geochim. Cosmochim. Acta* **69**, 5061 (2005).

72. S. Self, S. Blake, K. Sharma, M. Widdowson, S. Sephton, Sulfur and chlorine in late Cretaceous Deccan magmas and eruptive gas release. *Science* **319**, 1654 (2008).

73. R. von Glasow, Atmospheric chemistry in volcanic plumes. *Proc. Nat. Acad. Sci. U.S.A.* **107**, 6594 (Apr 13, 2010).

74. NOAA www.ncdc.noaa.gov/extremes/records/daily/maxt/2012/03/00?sts[]=US (2012)

75. World Ozone and Ultraviolet Radiation Data Center www.woudc.org/data_e.html (2012)

76. Environment Canada exp-studies.tor.ec.gc.ca/clf2/e/ozoneworld.html (2012)

77. P. Minnis *et al.*, Radiative climate forcing by the Mount Pinatubo eruption. *Science* **259**, 1411 (1993).

78. www.nefsc.noaa.gov/press_release/2012/SciSpot/SS1209/ (2012)

79. Global Volcanism Program www.volcano.si.edu/world/largeeruptions.cfm (2012)

80. en.wikipedia.org/wiki/Fluorescent_lamp (2012)

81. J. D. Haigh, A. R. Winning, R. Toumi, J. W. Harder, An influence of solar spectral variations on radiative forcing of climate. *Nature* **467**, 696 (Oct 7, 2010).

82. J. Knight *et al.*, in *State of the Climate in 2008*, T. C. Peterson, M. O. Baringer, Eds. (Bull. Am. Meteorol. Soc., 2009) vol. 90,pp. S22-S23.

83. www.oco.noaa.gov/index.jsp?show_page=page_roc.jsp&nav=universal (2012)

84. J. Hansen *et al.*, Climate response times: dependence on climate sensitivity and ocean mixing. *Science* **229**, 857 (1985).

85. C. M. Domingues *et al.*, Improved estimates of upper-ocean warming and multi-decadal sea-level rise. *Nature* **453**, 1090 (2008).

86. S. J. Smith *et al.*, Anthropogenic sulfur dioxide emissions: 1850–2005. *Atmos. Chem. Phys.* **11**, 1101 (2011).

87. ftp.cmdl.noaa.gov/ccg/co2/trends/co2_annmean_mlo.txt (2012)

88. K. E. Trenberth, An imperative for climate change planning: tracking Earth's global energy. *Curr. Opin. Environ. Sustain.* **1**, 19 (2009).

89. J. P. LaRiviere *et al.*, Late Miocene decoupling of oceanic warmth and atmospheric carbon dioxide forcing. *Nature* **486**, 97 (2012).

90. R. A. Berner, Phanerozoic atmospheric oxygen: New results using the GEOCARBSULF model. *Am. J. Sci.* **309**, 603 (2009).

91. D. Seidel, Q. Fu, W. RanDel, T. ReichleR, Widening of the tropical belt in a changing climate. *Nat. Geosci.* **1**, 21 (2008).

92. L. M. Polvani, D. W. Waugh, G. J. P. Correa, S. W. Son, Stratospheric ozone depletion: The main driver of twentieth-century atmospheric circulation changes in the Southern Hemisphere. *J. Clim.* **24**, 795 (2011).

93. S. W. Son, N. F. Tandon, L. M. Polvani, D. W. Waugh, Ozone hole and Southern Hemisphere climate change. *Geophys. Res. Lett* **36**, L15705 (2009).

94. R. J. Allen, S. C. Sherwood, J. R. Norris, C. S. Zender, Recent Northern Hemisphere tropical expansion primarily driven by black carbon and tropospheric ozone. *Nature* **485**, 350 (2012).

95. T. C. Bond, R. W. Bergstrom, Light absorption by carbonaceous particles: An investigative review. *Aerosol Sci. Tech.* **40**, 27 (2005).

96. M. Schnaiter *et al.*, UV-VIS-NIR spectral optical properties of soot and soot-containing aerosols. *J. Aerosol Sci.* **34**, 1421 (2003).

97. P. L. Ward, Sulfur dioxide initiates global climate change in four ways. *Thin Solid Films* **517**, 3188 (2009).

98. R. A. Rohde commons.wikimedia.org/wiki/File:Atmospheric_Transmission.png (2012)

99. www.epa.gov/air/emissions/ (2012)

100. R. D'Arrigo, R. Wilson, B. Liepert, P. Cherubini, On the 'Divergence Problem'in Northern Forests: A review of the tree-ring evidence and possible causes. *Global Planet. Change* **60**, 289 (2008).

101. T. Keller, Direct effects of sulphur dioxide on trees. *Phil. Trans. R. Soc. London, Ser. B* **305**, 317 (1984).

102. S. Manninen, S. Huttunen, Response of needle sulphur and nitrogen concentrations of Scots pine versus Norway spruce to SO_2 and NO_2. *Environ. Pollut.* **107**, 421 (2000).

103. R. Nemani *et al.*, Climate-driven increases in global terrestrial net primary production from 1982 to 1999. *Science* **300**, 1560 (2003).

104. T. C. Bond *et al.*, Historical emissions of black and organic carbon aerosol from energy-related combustion, 1850–2000. *Global Biogeochem. Cycles* **21**, GB2018 (2007).

105. T. Novakov *et al.*, Large historical changes of fossil-fuel black carbon aerosols. *Geophys. Res. Lett.* **30**, 1324 (2003).

106. E. J. Dlugokencky www.esrl.noaa.gov/gmd/aggi/aggi_2010.fig2.png (2010)

107. D. M. Etheridge, L. P. Steele, R. J. Francey, R. L. Langenfelds, Atmospheric methane between 1000 A.D. and present: Evidence of anthropogenic emissions and climatic variability *J. Geophys. Res.* **103**, 15979 (1998).

108. E. J. Dlugokencky *et al.*, Observational constraints on recent increases in the atmospheric CH_4 burden. *Geophys. Res. Lett.* **36**, L18803 (2009).

109. M. Aydin *et al.*, Recent decreases in fossil-fuel emissions of ethane and methane derived from firn air. *Nature* **476**, 198 (2011).

110. F. M. Kai, S. C. Tyler, J. T. Randerson, D. R. Blake, Reduced methane growth rate explained by decreased Northern Hemisphere microbial sources. *Nature* **476**, 194 (2011).

111. M. Schultz, S. Rast, *REanalysis of the TROpospheric chemical composition over the past 40 years*, retro.enes.org/reports/D1-6_final.pdf (2008).

112. U. S. Environmental Protection Agency, *National Air Pollutant Emission Trends, 1900 - 1998* www.epa.gov/ttnchie1/trends/trends98/ (2000), pp. 238.

113. J. Cofala, P. Rafaj, W. Schöpp, Z. Klimont, M. Amann worldenergyoutlook.org/docs/Emissions_of_Air_Pollutants_for_WEO2009.pdf (2009)

114. Y. Wang, D. J. Jacob, Anthropogenic forcing on tropospheric ozone and OH since preindustrial times. *J. Geophys. Res.* **D23**, 31123 (1998).

115. T. Staffelbach, A. Neftel, B. Stauffer, D. Jacob, Formaldehyde in polar ice cores: a possibility to characterize the atmospheric sink of methane in the past. *Nature* **349**, 603 (1991).

116. P. Bousquet, D. A. Hauglustaine, P. Peylin, C. Carouge, P. Ciais, Two decades of OH variability as inferred by an inversion of atmospheric transport and chemistry of methyl chloroform. *Atmos. Chem. Phys.* **5**, 1679 (2005).

117. R. Zander, P. Demoulin, D. Ehhalt, U. Schmidt, C. Rinsland, Secular increase of the total vertical column abundance of carbon monoxide above central Europe since 1950. *J. Geophys. Res.* **94**, 11021 (1989).

118. B. N. Duncan *et al.*, Global budget of CO, 1988–1997: Source estimates and validation with a global model. *J. Geophys. Res.* **112**, D22301 (2007).

119. W. J. Randel, F. Wu, H. Vömel, G. E. Nedoluha, P. Forster, Decreases in stratospheric water vapor after 2001: Links to changes in the tropical tropopause and the Brewer-Dobson circulation. *J. Geophys. Res.* **111**, D12312 (2006).

120. S. Solomon *et al.*, Contributions of stratospheric water vapor to decadal changes in the rate of global warming. *Science* **327**, 1219 (2010).

121. M. Wild, Global dimming and brightening: A review. *J. Geophys. Res.* **114**, D00D16 (2009).

122. Z. Lu *et al.*, Sulfur dioxide emissions in China and sulfur trends in East Asia since 2000. *Atmos. Chem. Phys.* **10**, 8657 (2010).

123. D. M. Etheridge *et al.* cdiac.ornl.gov/ftp/trends/co2/lawdome.combined.dat (1998)

124. NOAA ESRL www.esrl.noaa.gov/gmd/ccgg/trends/#mlo_full (2010)

125. K. Trenberth, J. Fasullo, Tracking Earth's Energy. *Science* **328**, 316 (2010).

126. J. Hansen *et al.*, Earth's energy imbalance: Confirmation and implications. *Science* **308**, 1431 (2005).

127. G. A. Zielinski, P. A. Mayewski, L. D. Meeker, S. Whitlow, M. Twickler, A 110,000-year record of explosive volcanism from the GISP2 (Greenland) ice core. *Quat. Res.* **45**, 109 (1996) (ftp.ncdc.noaa.gov/pub/data/paleo/icecore/greenland/summit/gisp2/chem/volcano.txt).

128. J. W. C. White *et al.*, The climate signal in the stable isotopes of snow from Summit, Greenland: Results of comparisons with modern climate observations. *J. Geophys. Res.* **102**, 26425 (1997) (ftp.ncdc.noaa.gov/pub/data/paleo/icecore/greenland/summit/gisp2/isotopes/stacked.txt).

129. P. A. Mayewski *et al.*, Major features and forcing of high-latitude northern hemisphere atmospheric circulation using a 110,000-year-long glaciochemical series. *J. Geophys. Res.* **102**, 26345 (1997).

130. L. Barrie, R. Hoff, S. Daggupaty, The influence of mid-latitudinal pollution sources on haze in the Canadian Arctic. *Atmos. Environ.* **15**, 1407 (1981).

131. G. C. Hegerl *et al.*, Detection of human influence on a new, validated 1500-year temperature reconstruction. *J. Clim.* **20**, 650 (2007).

132. G. J. S. Bluth, S. D. Doiron, C. C. Schnetzler, A. J. Krueger, L. S. Walter, Global tracking of the SO_2 clouds from the June, 1991 Mount Pinatubo eruptions. *Geophys. Res. Lett.* **19**, 151 (1992).

133. R. S. Stone, J. Keys, E. G. Dutton, Properties and decay of stratospheric aerosols in the Arctic following the 1991 eruptions of Mount Pinatubo. *Geophys. Res. Lett.* **20**, 2539 (1993).

134. D. W. Lea, Climate Impact of Late Quaternary Equatorial Pacific Sea Surface Temperature Variations. *Science* **289**, 1719 (2000).

135. S. Self, J.-X. Zhao, R. E. Holasek, R. C. Torres, A. J. King, in *Fire and Mud: Eruptions and lahars of Mount Pinatubo, Philippines*, C. G. Newhall, R. S. Punongbayan, Eds. (Philippine Institute of Volcanology and Seismology and University of Washington Press, 1996) pp. 1089-1115.

136. G. Stenchikov *et al.*, Arctic Oscillation response to volcanic eruptions in the IPCC AR4 climate models. *J. Geophys. Res.* **111**, D07107 (2006).

137. P. J. Gleckler *et al.*, Krakatoa's signature persists in the ocean. *Nature* **439**, 675 (2006).

138. J. M. Gregory, J. A. Lowe, S. F. B. Tett, Simulated global-mean sea level changes over the last half-millennium. *J. Clim.* **19**, 4576 (2006).

139. V. Fiedler *et al.*, East Asian SO_2 pollution plume over Europe–Part 1: Airborne trace gas measurements and source identification by particle dispersion model simulations. *Atmos. Chem. Phys.* **9**, 4717 (2009).

140. V. Fiedler *et al.*, East Asian SO_2 pollution plume over Europe-Part 2: Evolution and potential impact. *Atmos. Chem. Phys.* **9**, 4729 (2009).

141. T. Thordarson, S. Self, Atmospheric and environmental effects of the 1783–1784 Laki eruption: A review and reassessment. *J. Geophys. Res.* **108**, 4011 (2003).

142. P. L. Ward, Understanding volcanoes may be the key to controlling global warming. *Soc. Vac. Coaters Bull.* **Summer**, 26 (2010).

143. T. Thordarson, S. Self, N. Oskarsson, T. Hulsebosch, Sulfur, chlorine, and fluorine degassing and atmospheric loading by the 1783–1784 AD Laki (Skaftár Fires) eruption in Iceland. *Bull. Volcanol.* **58**, 205 (1996).

144. J. M. Licciardi, M. D. Kurz, J. M. Curtice, Glacial and volcanic history of Icelandic table mountains from cosmogenic 3He exposure ages. *Quat. Sci. Rev.* **26**, 1529 (2007).

145. S. Rahmstorf, Timing of abrupt climate change: A precise clock. *Geophys. Res. Lett.* **30**, 1510 (2003).

146. J. P. Severinghaus, Abrupt climate change at the end of the last glacial period inferred from trapped air in polar ice. *Science* **286**, 930 (1999).

147. R. D. Norris, U. Rohl, Carbon cycling and chronology of climatewarming during the Palaeocene/Eocene transition. *Nature* **401**, 775 (1999).

148. V. E. Courtillot, P. R. Renne, On the ages of flood basalt events. *C.R. Geosci.* **335**, 113 (2003).

149. **P. Wignall**, The link between large igneous province eruptions and mass extinctions. *Elements* **1**, 293 (2005).

150. en.wikipedia.org/wiki/Siberian_Traps (2012)

151. H. Visscher *et al.*, Environmental mutagenesis during the end-Permian ecological crisis. *Proc. Nat. Acad. Sci. U.S.A.* **101**, 12952 (2004).

152. J.-P. Cogné, E. Humler, Trends and rhythms in global seafloor generation rate. *Geochemistry Geophysics Geosystems* **7**, Q03011 (2006).

153. F. Sigmundsson *et al.*, Intrusion triggering of the 2010 Eyjafjallajökull explosive eruption. *Nature* **468**, 426 (2010).

154. D. De Muer, H. De Backer, Revision of 20 years of Dobson total ozone data at Uccle (Belgium): Fictitious Dobson total ozone trends induced by sulfur dioxide trends. *J. Geophys. Res.* **97**, 5921 (1992).

155. C. T. A. Lee, P. Luffi, T. Plank, H. Dalton, W. P. Leeman, Constraints on the depths and temperatures of basaltic magma generation on Earth and other terrestrial planets using new thermobarometers for mafic magmas. *Earth Planet. Sci. Lett.* **279**, 20 (2009).

156. S. Thorarinsson, G. Sigvaldason, The Hekla eruption of 1970. *Bull. Volcanol.* **36**, 269 (1972).

157. S. Thorarinsson, *Hekla: A notorius volcano* (Almenna Bokafelagid, Reykjavik, 1970), pp. 54.

158. E. Cordero, P. A. Newman, C. Weaver, E. Fleming www.ccpo.odu.edu/~lizsmith/SEES/ozone/class/Chap_6/index.htm (2012)